Review

Electromagnetic Wave Tailoring: From One Dimension to Multiple Dimensions

Jing Cheng Zhang[1,2], Geng-Bo Wu[1,2], Mu Ku Chen[1,2,3], Xiaoyu Che[1,2], Yao Liang[1,2], Din Ping Tsai[1,2,3], and Chi Hou Chan[1,2]

1. *Department of Electrical Engineering, City University of Hong Kong, Hong Kong SAR 999077, China*
2. *State Key Laboratory of Terahertz and Millimeter Waves, City University of Hong Kong, Hong Kong SAR 999077, China*
3. *Centre for Biosystems, Neuroscience, and Nanotechnology, City University of Hong Kong, Hong Kong SAR 999077, China*

Jing Cheng Zhang , Geng-Bo Wu , and Mu Ku Chen contributed equally.
Corresponding authors: Din Ping Tsai, Email: dptsai@cityu.edu.hk; Chi Hou Chan, Email: eechic@cityu.edu.hk.
Received April 26, 2023; Accepted July 21, 2023; Published Online August 9, 2023.

Abstract — Metasurfaces, known as arrays of subwavelength antennas, provide a wide range of options for controlling electromagnetic waves and effectively reducing the size and complexity of electromagnetic devices. Metasurfaces can manipulate five degrees of freedom of electromagnetic waves: amplitude, wavelength, polarization, phase, and orbital angular momentum; these are customized to provide a variety of remarkable functionalities, including metalenses and meta-holograms. With the advancement of simultaneously manipulating two or more degrees of freedom of the electromagnetic field, there has been a significant increase in the amount of information that electromagnetic waves can carry. The wavefront can be precisely tailored for specific applications, facilitating new possibilities for innovative applications with high performance and diverse functionalities, such as full-color vectorial meta-holograms achieved by a single-layer metasurface. This review briefly overviews the latest developments in metasurfaces, categorizing them based on their various degrees of freedom used to manipulate the electromagnetic waves. The use of metasurfaces to control electromagnetic waves from one dimension to multiple dimensions is systematically explored. The challenges and opportunities for future research are discussed.

Keywords — Electromagnetic wave manipulation, Metasurfaces, Single-dimensional manipulation, Multidimensional manipulation.

Citation — Jing Cheng Zhang, Geng-Bo Wu, Mu Ku Chen, *et al.*, "Electromagnetic Wave Tailoring: From One Dimension to Multiple Dimensions," *Electromagnetic Science*, vol. 1, no. 3, article no. 0030131, 2023. doi: 10.23919/emsci.2023.0013.

I. Introduction

Humans have been exploring the properties of light for centuries, with significant contributions made by pioneers, such as Mozi and Aristotle. Mozi proposed that "light travels in straight lines" and discovered the principle of pinhole imaging. Aristotle studied the refraction and reflection of light, providing essential contributions to optics. As our understanding of light continues to deepen, light has become known as the electromagnetic (EM) wave and has led to the development of new technologies and applications in fields, such as communications, imaging, and material analysis.

EM waves exhibit distinct properties that provide them with unique applications in various fields. For instance, microwaves are extensively utilized for communications, broadcasting, and navigation due to their ability to penetrate buildings and obstacles while transmitting information over long distances [1]–[3]. Terahertz waves have unique properties, including remarkable penetration, high imaging resolution, and little biological damage, making them ideal for applications in nondestructive testing, securi-

ty inspection, biomedical diagnosis, high-speed wireless communications, and material analysis [4]–[6]. Visible light is used for illumination, photography, imaging, laser technology, and other applications [7]. This ongoing process has shown the potential use of EM waves.

The functionalities of EM devices, such as filters, modulators, and lenses, are explored by manipulating different degrees of freedom of EM waves, including amplitude, frequency, polarization, phase, and orbital angular momentum (OAM). The size and weight of traditional devices impede the miniaturization and integration of EM systems. There is an ever-increasing demand for cutting-edge methodologies that can effectively manipulate EM waves in diverse dimensions and design EM devices to cater to unique requirements.

A metasurface is an ultrathin planar structure composed of subwavelength elements that manipulate the amplitude, phase, wavelength, polarization, and orbital angular momentum of EM waves [8]–[16]. It has emerged as a powerful platform for effectively performing various func-

tions [17]–[20]. With the continuous advancement of micro- and nano-fabrication technologies, including electron beam lithography [21]–[23] and 3D printing [24]–[27], metasurfaces with micro-nano structures and complex shapes can be fabricated by advanced fabrication techniques. The involvement of new materials, such as dielectric materials [28], phase change materials [29], and diodes [30], with advanced design methods, such as integrated resonant unit elements (IRUEs) [31], enhances the EM wave control ability of metasurfaces in multiple dimensions.

In this article, we summarize the latest progress in manipulating EM waves with metasurfaces from one dimension to multiple dimensions. Research in this field is highly important. A classification from a recent study based on the different dimensions utilized to manipulate electromagnetic waves is presented (Figure 1). This review highlights the growing trend of metasurfaces in achieving more efficient multidimensional manipulation of EM waves. Section II focuses on using metasurfaces to manipulate EM waves in a single dimension. Section III delves deeper into EM manipulation using metasurfaces in two or more dimensions. In the concluding section, we propose our viewpoints on the challenges and potential opportunities involved in the multidimensional manipulation of EM waves.
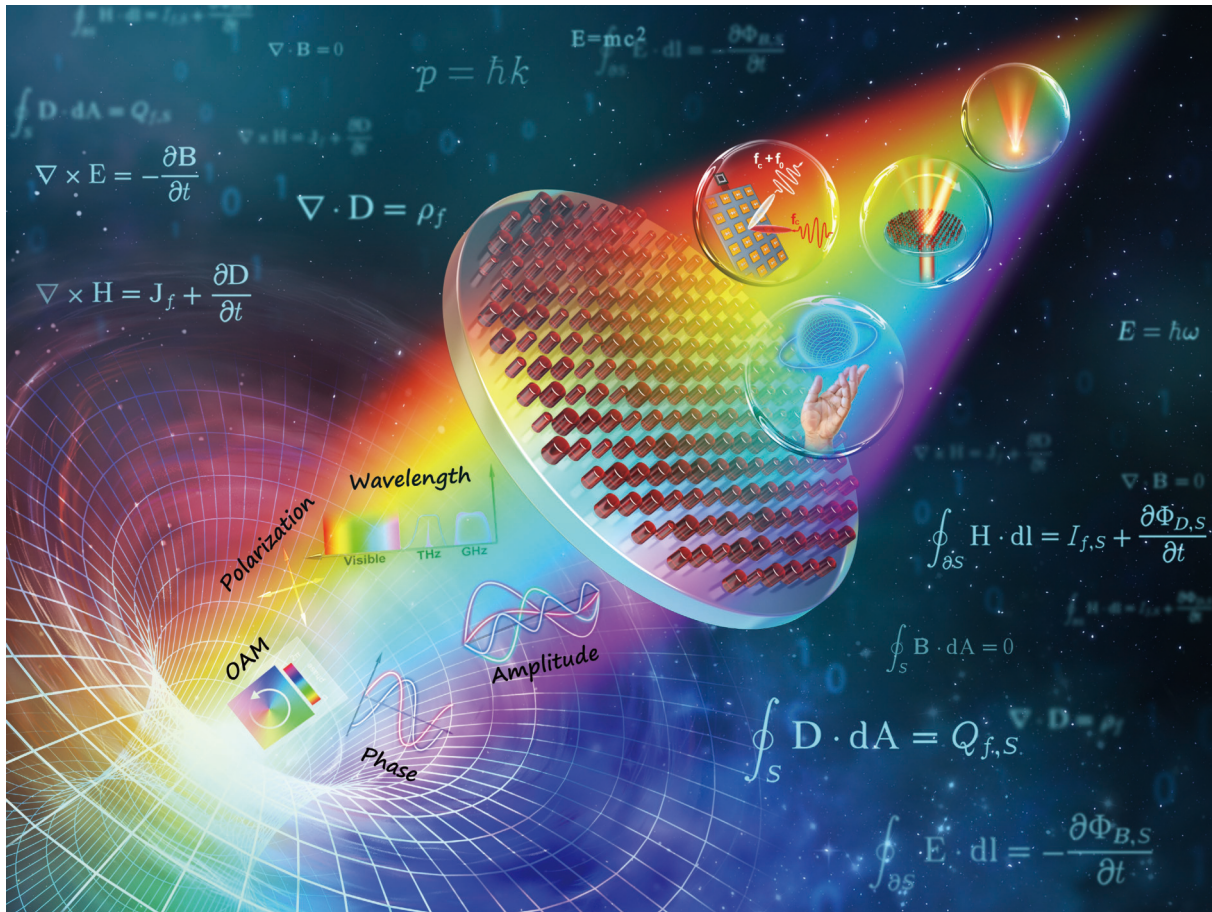
Figure 1 Schematic of the various applications achieved by metasurfaces, showcasing the ability to tune multiple degrees of freedom (DOFs) of electromagnetic waves.

II. EM Wave Tailoring in One Dimension

Metasurfaces perform as an excellent platform for tailoring electromagnetic waves. They can effectively manipulate electromagnetic waves with arbitrary degrees of freedom (DOFs) [32]–[37]. The DOFs include phases, polarizations, amplitudes, wavelengths, and orbital angular momentums. Researchers have extensively investigated and explored practical ways to modulate EM waves in the past decade. This section briefly elaborates on the typical approaches developed in recent years to manipulate EM waves in one dimension with metasurfaces.

1. Phase

Focusing electromagnetic waves has been a fundamental demand from ancient to modern times. People used crystal lenses to focus sunrays onto ignitable materials for lighting fires in the 11th and 12th centuries. Currently, lenses have much more widespread applications, such as cameras, telescopes, and microscopes. These traditional lenses modulate the phase of light by accumulating phase shifts along the optical paths, which are determined by the shape and material of the lenses. Traditional methods have a few restrictions, such as monochromatic and chromatic aberrations. The combination of multiple lenses and specialized design

methods can minimize these aberrations. This design results in a rapid increase in the size of the bulk lenses.

Metalens [38]–[43], as the most representative branch of the metasurface, has the potential to revolutionize optics by enabling a compact, lightweight flat lenses. However, the chromatic aberration still degrades the performance of the metalens when it is designed at a single wavelength.

Tsai's group overcame this challenging problem. They demonstrated the first broadband achromatic metalens operating in reflection mode with a continuous wavelength range from 1200 to 1680 nm [44]. Each unit cell consisted of one or more metallic nanoantennas, working as IRUEs [31] to compensate for the phase in different wavelengths. This innovative design enabled precise control of phase dispersion, which significantly promoted the development of meta-devices for full-color control, ultimately leading to

practical applications [45].

The design with IRUEs paved the way to address the challenge of color imaging and display in the field of flat optics. This group also demonstrated a broadband achromatic metalens in the visible band [46]. The metalens was composed of gallium nitride nanopillars, and the diameter was 50 μm. This was the first study to capture a full-color image using a metalens. Figure 2(a) illustrates several examples of achromatic metalenses. The combination of the Pancharatnam-Berry (PB) and propagation phases achieved the IRUE used here. The PB phase was responsible for the phase requirement of the maximum wavelength. The propagation phase compensated for the phase dispersions to form perfect focusing phase profiles for all wavelengths.

This revolutionary advance caused optical devices to be more compact and have superior performances. For ex-
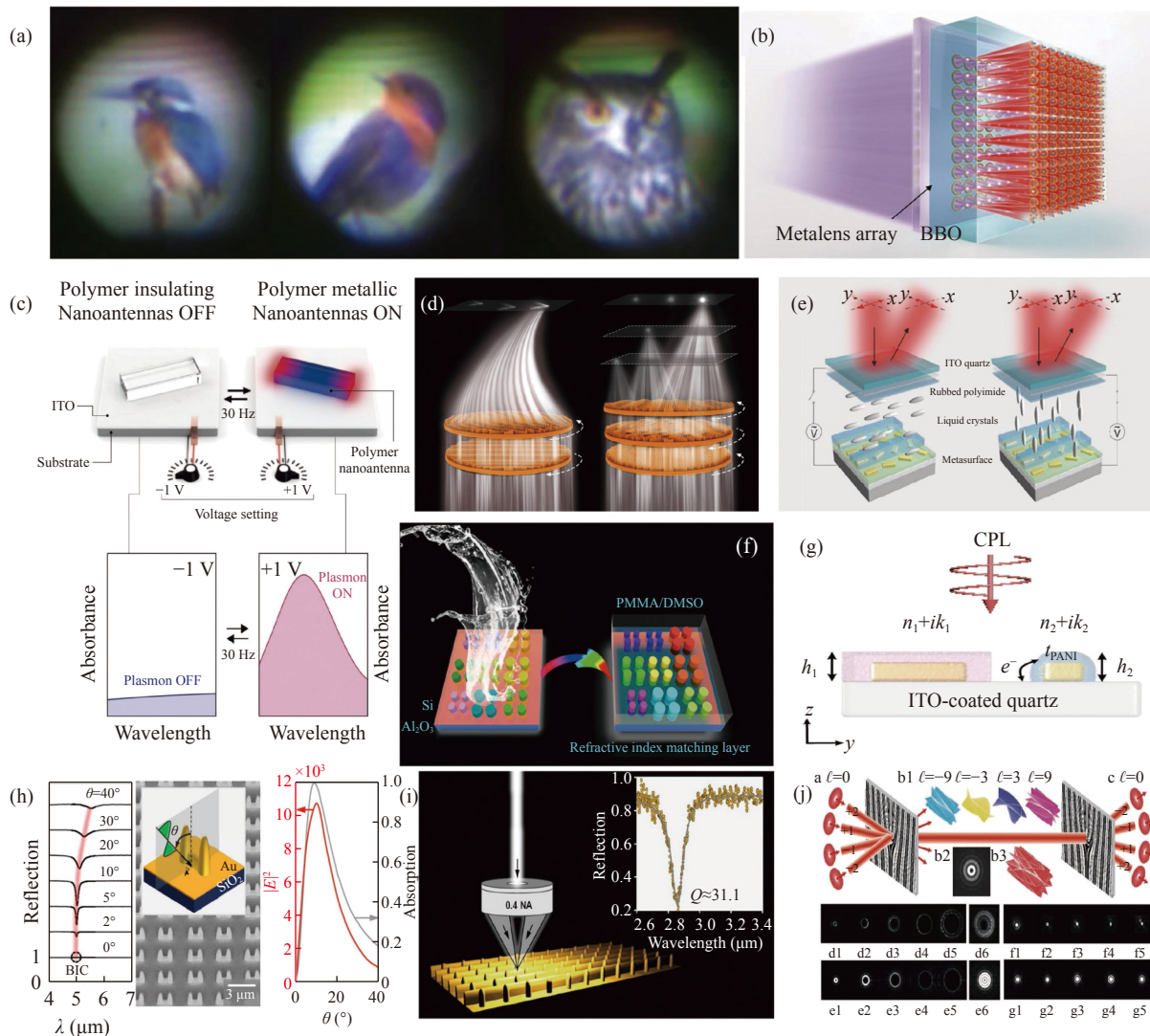
Figure 2 Single-dimensional manipulation of EM waves with metasurfaces. (a) Full-color images captured by the broadband achromatic metalens [46]; (b) Multidimensional quantum source based on the meta-lens array [47]; (c) Electrically switchable metallic polymer nanoantennas [48]; (d) Varifocal meta-devices for the next-generation communication systems [9]; (e) Electrically tunable optical metasurfaces for dynamic polarization conversion [49]; (f) All-dielectric metasurface for high-performance structural color [50]; (g) Electrochemically controlled metasurfaces with high contrast switching [51]; (h) Metamaterial absorbers enabled by the physics of bound states in the continuum [52]; (i) Over 80% absorption enabled by the flat-band and bound states in the continuum mechanism [53]; (j) Orbital angular momentum multiplexing for optical communications [54].

ample, an achromatic metalens array can work as a full-color light-field camera and reconstruct images with different depths of focus [55]. The metalens array can also be used as a high-dimensional quantum source (Figure 2(b)) [47]. The ten-by-ten metalens array can generate a 100-path spontaneous parametric down-conversion photo-pair source. The advanced quantum source is achieved by integrating the metalens array with a 0.5-mm type II b-barium borate (BBO) crystal. The focal spots are generated inside the BBO crystal, trigger the spontaneous parametric down-conversion process, and generate 100 pairs of entangled photonic sources. Thus, metalens array have become a novel and essential platform for quantum devices [13].

Most metasurfaces are passive, and once manufactured, their optical function remains static. For example, the metalens always focuses the light on the same focal spot. The active metasurface, which could dynamically adjust the optical phase features, thus caused widespread interest. Giessen *et al.* demonstrated a novel electrochemical method to control the phase of the nanoantenna at up to 30 hertz (Figure 2(c)) [48]. The polymer metasurface could actively steer the beam, whereas the nanoantenna was composed of a polymer with optical metallic properties. When a voltage of +1 V was applied through indium tin oxide (ITO), the polymer nanoantenna was electrochemically doped and oxidized. The oxidized nanoantenna showed a strong plasmonic resonance in the near-infrared (IR) spectral range. Thus, the nanoantenna could work with the PB phase, manipulating incident light on demand. When the voltage was switched to −1 V, the nanoantenna turned into an insulator and could not modulate the incident beam. This method was low cost compared with commercial polymers and could expand the functions of electro-optical active devices. The polymer metasurface was much easier to fabricate on curved devices or flexible substrates, significantly promoting the development of virtual and augmented reality innovations. Energy savings were another advantage of the electrochemically driven metasurface, as the 1 V voltage amplitude was sufficient.

Cascading multiple metasurfaces can expand the wave manipulation capability, providing extra degrees of freedom, i.e., mutual rotation or displacement [56]. Chan *et al.* demonstrated two kinds of terahertz (THz) varifocal meta-devices. The THz beams could be projected into any spot in a 2D plane or 3D space (Figure 2(d)) [9]. The generation and manipulation of the THz Airy beam were also demonstrated. The working principle was that two gradient phase profiles and two focusing phase profiles were distributed onto separate metasurfaces that could be mutually rotated. Then, a tunable total phase profile of the separate metasurfaces was achieved by incorporating and superimposing multiple phase profiles, such as the cubic phase, gradient phases, and focusing phases, to achieve tunable beam steering and a tunable focal spot in a 3D space. The proposed meta-device was manufactured using low-cost 3D printing and was suitable for large-scale processing. This THz vari-focal meta-devices could securely, flexibly, and stably transmit signals.

These pioneering metasurfaces with phase control based on different mechanisms, such as the resonant phase [19], PB phase [55], propagation phase [56], and chiral meta-atom-induced phase [57], have facilitated the miniaturization of the free-space EM elements and enabled numerous practical applications, such as meta-hologram and optical encryption [58].

2. Polarization

Traditional bulky optical elements, such as the half-wave plates, linear polarizers, and polarization beam splitters, have long performed polarization generation and manipulation. They work well but are bulky and not suitable for miniaturized systems.

Many efforts have been made to develop meta-devices for generating and manipulating polarization states. Tsai *et al.* demonstrated a multiple polarization state generator [59]. The chip could generate four reflected linear polarizations (horizontal, vertical, +45°, and −45°) and two circular polarizations under linear polarization incidence. This generator was composed of aluminum nanoantennas; hence, the thin chip was capable of working in the entire visible band. The nearby supercells were designed to reflect the two circular beams in opposite directions according to the PB phase principle. Thus, there were two circular polarization components in each direction, and they had a beam superposition. Therefore, different polarization states could be generated by modulating the phase difference of the two circular polarizations.

As the transmission mode is also essential for flat optics, Luo *et al.* developed an all-dielectric polarization generator working in the mid-infrared band [60]. Xiao *et al.* demonstrated a metasurface-based all-in-one entire Poincaré sphere polarizer whose working wavelength was 633 nm [61]. This approach facilitated the selective transfer and transformation of a specific polarization orientation at any point on the Poincaré sphere into its mirror image while entirely obstructing the perpendicular orientation.

Active polarization manipulation is highly desirable in many optical applications, including optical communications, information processing, and sensing. Singh *et al.* demonstrated an all-optical controlled polarization switch working for THz waves [62]. The polarization states could be switched in a very short time of approximately 667 fs. The meta-antenna consisted of an aluminum split ring and a silicon ring below the sapphire substrate. The split gap induced different resonance behaviors for different polarizations. The change in the silicon properties further modulated the output polarization. When an 800 nm pulsed laser was incident on the silicon ring, the photoconductivity of the silicon film was enhanced, leading to a change in the co- and cross-polarized transmission. These transmissions defined the final output polarization. This meta-device was useful for ultrafast data encoding and polarization-division multiplexing in terahertz wireless communications.

Atwater *et al.* demonstrated a meta-device for the near-infrared band for dynamic polarization conversion [63]. The proposed meta-device could convert the incident *y*-polarized beam to a reflected *x*-polarized, elliptically polarized, or circular polarized beam depending on the bias voltage, which could modulate the refractive index of indium tin oxide.

On the other hand, Liu *et al.* made a breakthrough in dynamic polarization conversion within the visible spectrum (Figure 2(e)) [49]. Their metasurface consisted of gold nanoantennas, which were enfolded into a layer of liquid crystal or polymethyl methacrylate (PMMA) row by row. The gold nanorods were surrounded with a thin dielectric polymer to eliminate the effect of the refractive index change of the liquid crystals. The metasurface was placed on an ITO-coated glass/silicon substrate, working as one of the electrodes. The ITO-coated quartz superstructure was the other electrode. Thus, the refractive index of the surrounding liquid crystals could be tuned by the biased voltage applied to the ITO layers. Based on the PB phase principle, the two well-defined nearby rows reflected the two circular polarization waves. One was from the liquid crystal-coated part, and the other was from the PMMA-coated part. Their superimposition defined the final polarization state depending on the phase differences between the two regions. The phase difference could be tuned through the refractive index change of the liquid crystals coated on the nanorods under the biased voltage, while the PMMA's refractive index did not change. The linear polarization could be rotated up to 90 degrees resulting from the phase differences. The metasurface's ability to dynamically rotate polarization was exceptional, as it remained fully reversible for up to 100 cycles without any substantial decline in performance. Moreover, the measured switching speed was approximately 100 ms, indicating its fast and efficient operation.

Recently, Wang *et al.* conducted a study and discovered that the introduction of engineered noise into the meta-hologram resulted in an enhanced storage capacity of up to 11 independent holographic images. This methodology has great potential for metasurfaces in various applications, including high-capacity optical displays, information encryption, and data storage [64].

3. Wavelength

Precise control of the wavelengths by a metasurface contributes to the development of various optical applications, such as nonlinear optics [65]–[68] and structural color [69]–[71]. Traditional nonlinear crystals suffer from poor thermal stability and small nonlinear coefficients [72], [73]. Furthermore, nonlinear optical crystals that can excite second harmonic generation in the vacuum ultraviolet (VUV) spectral region are rare. Metasurfaces provide a compact and efficient approach to induce nonlinear effects and achieve straightforward coherent VUV light generation. Halas *et al.* demonstrated second harmonic generation (SHG) using an all-dielectric metasurface [16]. The meta-surface was composed of zinc oxide nanoantennas. The nanoantenna was optimized for facilitating resonance, specifically at a wavelength of 394 nm. The confinement of incident energy within the material by magnetic resonance enabled the efficient generation of SHG in bulk due to the nonlinear properties of zinc oxide. When subjected to nearly normal incident illumination, the resonant metasurface greatly enhanced the SHG dramatically with a wavelength of 197 nm. The compact device could easily be integrated into laser systems for VUV light sources without complex experimental configurations or phase matching.

For linear optics, the metasurface can produce vivid colors through the orientations or dimensions of nanoantennas. The color generation method addresses environmental issues, such as pigment-induced pollution, and improves color stability and mechanical durability. Song *et al.* demonstrated the utilization of electric and magnetic resonances in TiO_2 metasurfaces to achieve high-resolution, low-loss, and all-dielectric structural colors [74]. The proposed metasurface was a square lattice of nanoblocks. The spatial resolution could achieve approximately 16000 dpi when there was only a four by four nanoblock array.

However, achieving structural color in large gamut, high saturation, high brightness, and high resolution is still challenging. Xiao *et al.* overcame this challenge [50]. Their solution was to add a refractive index matching layer, i.e., PMMA or dimethyl sulfoxide (DMSO), onto the silicon metasurface (Figure 2(f)). Thus, the brightness and color purity were significantly improved by reducing both the reflection bandwidth and background reflection. The active tuning of structural colors was essential for practical applications. Rho *et al.* experimentally demonstrated an electrically tunable color printing metasurface [75]. The silicon metasurface was embedded with a layer of LCs. The application of a biased voltage caused the orientation of the LC molecules to change, resulting in an altered refractive index. Subsequently, the orientation change induced a shift in resonance and ultimately caused a difference in the displayed color. This development was a significant stride toward the achievement of structural color-based displays.

4. Amplitude

The change in amplitude of electromagnetic waves is a crucial mechanism for conveying information. This topic can be broadly divided into nonresonance and resonance amplitude changes.

Nonresonance-based amplitude changes involve modifying the electromagnetic wave's intensity without relying on resonance effects. Recent representative work was led by Liu *et al.*; they demonstrated a chemically controlled metasurface hologram with high-contrast switching at visible frequencies by locally conjugating preselected antennas with a conducting polymer and polyaniline [51], as shown in Figure 2(g). The optical responses of the metasurfaces could be modulated by controlling the polyaniline thickness during electrochemical growth, and the operation of the metasurfaces was electrochemically powered.

On the other hand, resonance-based amplitude changes are highly relevant in metamaterial absorbers, which can efficiently absorb light energy and convert it into other forms of energy, such as thermal, chemical, or electronic energy [76], [77]. This absorption process is often facilitated by localized or nonlocalized plasmon resonances [78], [79], resulting from the electrons' collective oscillations in the metamaterial's structure.

The resonance amplitude of metamaterial absorbers with a single resonance is customized by adjusting the metamaterial's geometry, composition, and oblique incident angle of excitation [52], [80]–[84]. These adjustments modify the ratio of radiation loss (γ_{rad}) to dissipation loss (γ_{dis}) of the resonance, resulting in resonance amplitude changes. For instance, with metamaterial absorbers that utilize the physics of bound states in the continuum and consist of vertical split-ring resonators on the metal surfaces (Figure 2(h)), increasing the oblique incident angle enhances radiation loss, leading to under coupling ($\gamma_{rad} < \gamma_{dis}$), critical coupling ($\gamma_{rad} = \gamma_{dis}$), and over coupling ($\gamma_{rad} > \gamma_{dis}$) regimes. Remarkably, perfect absorption occurs at the critical coupling condition (an oblique incident angle of approximately 10°), resulting in a maximum light field enhancement (over 10^4) in the mid-infrared (mid-IR) regime [52]. Furthermore, the spectral linewidth of the resonance also affects near-field enhancement, with narrower linewidths yielding better enhancement at similar resonance amplitudes (Figure 2(h)).

Molecular fingerprint detection identifies molecules based on their unique absorption spectra in the mid-IR region. Plasmonic metamaterial absorbers generate an enhanced field that improves the sensitivity and accuracy of this detection process, enabling more precise identification of molecules. A recent study demonstrated that plasmonic metamaterial absorbers could exhibit different amplitude modulations when coated with thin PMMA films as an analyte, depending on the coupling regime. Specifically, under coupling led to a reduction in the resonance peak, critical coupling led to no change, and over-coupling led to an increase in the resonance peak. This novel property was crucial for amplitude-modulated sensing [85], [86].

Interfacial engineering is an effective method to modulate the resonance amplitude in metasurfaces. Odom et al. proposed that coating a thin 2D material film on a metasurface could produce the resonance depth of the plasmonic surface lattice resonances (SLRs) [87], [88].

Controlling the angular dispersion of metamaterial absorbers is crucial to simultaneously achieve a strong resonance depth and narrow linewidth when using focused beams as excitation [89]. A recent study led by Kivshar et al. demonstrated that using flat-band physics and bound states in the continuum mechanism achieved sharp resonances (Q > 30) with over 80% absorption in plasmonic metasurfaces [53], as depicted in Figure 2(i).

These resonant absorbers with amplitude control have enabled numerous practical applications, including solar energy harvesting [90], plasmon-enhanced infrared spectroscopy [91], lasing [92], structural color display [93], and thermal imaging [94].

5. Orbital angular momentum (OAM)

Since its discovery, OAM has become a topic of growing interest [95], [96] and has been explored as an important DOF in optical applications. Wang et al. demonstrated optical communication using four OAM states multiplexing and greatly enhanced the capacity of free space communications [97]. They also showed that the information-carrying ability was further enhanced when combining the OAM with other DOFs, such as polarization and wavelength. The experiment used four spatial light modulators to convert Gaussian beams into OAM beams and back into Gaussian beams. OAM multiplexing at RF frequencies was also demonstrated using a holographic metasurface antenna [98], which could suppress undesired residual OAM modes in free space. To make the configuration more compact, Yuan et al. demonstrated optical OAM multiplexing communications using two Dammann optical vortex gratings (Figure 2(j)) [54]. One converted the Gaussian beams of different incident angles to OAM beams of the same transmission route. The other was used for demultiplexing the OAM beams back and using ten OAM states, eighty wavelengths, and two polarization states to build a communication system with 1600 independent information channels. The Dammann optical vortex grating eliminated the obstacle of multiple OAM state generation and detection simultaneously. It was a promising prospect to enhance the capacity of optical communication systems up to the level of Pbit/s. Most OAM launchers could only generate fixed OAM modes. A mode-reconfigurable metasurface doublet was demonstrated [99]. By in-plane rotation of the upper metasurface with different angles, the generated OAM mode number could be switched among 0, ±1, and ±2.

In addition to increasing the optical communication capacity, OAM multiplexing could be used to design varifocal metalenses [100]. The focal lengths were tuned from 5 mm to 35 mm, depending on the OAM state of the incident beam. The principle was to design several OAM-related metalenses and combine them in an interlaced arrangement. On the other hand, Luo et al. demonstrated an angular metalens that could manipulate the focal spot in the same focal plane [101]. The focusing phase profile was achieved by adding the phase profile of the incident OAM beam with the azimuthal-quadratic phase profile coded on the metasurface.

The main challenge for applying OAM at RF frequencies is the inherent divergence property of vortex waves. An electrically large receiving antenna is required to capture most of the OAM energy at the receiver end. A higher-order Bessel beam incorporating a Bessel beam and OAM beam was proposed to generate nondiffractive OAM waves [4]. It was further extended to an extended higher-order Bessel beam that could focus the OAM energy in a tailor-made longitudinal region by optimizing the phase profile of

the metasurface.

Advancements in OAM research have driven progress in numerous applications [102]. For example, OAM has been used in communication systems to improve data transfer rates, network capacity, imaging resolution, and imaging sensitivity. Additionally, OAM has been applied in fields such as quantum computing, laser machining, and optical trapping, among others. The continued advancements in OAM research will lead to increasingly innovative applications.

III. EM Wave Tailoring in Multiple Dimensions Simultaneously

The methods discussed in Section II focus predominantly on one-dimensional EM wave manipulation and the achievement of single optical functionality, which needs to be enhanced to develop customized optical devices. Presently, researchers in this field are directing their efforts toward the performance enhancement of EM devices based on metasurfaces and achieving integrated, multifunctional EM devices through the multidimensional manipulation of EM waves with metasurfaces. This section provides a general discussion of current research on the multiple-dimensional manipulations of EM waves with metasurfaces.

1. Polarization and wavelength

The unique frequency-dependent absorption and transmission properties for different polarization incidences will lead to critical practical applications for linear optics. One typical example is to achieve structural coloration artworks featuring photorealistic and stereoscopic impressions [103]. The color hue and brightness can be independently controlled by the geometric scaling factor and orientation of the nanoaperture in a surface-relief plasmonic metasurface, respectively. Moreover, by leveraging the polarization diversities of the incident and reflected lights, the metasurface can achieve kaleidoscopic steganography that presents multiple images with different polarizer-analyzer combinations.

Photonic bound states in the continuum (BICs) enable infinite quality factor resonances due to the elimination of radiation loss [104]–[108]. In practice, only quasi-BICs with strong local field enhancement and a high Q-factor are available considering the imperfect fabrication, finite-size effects, etc. Quasi-BICs provide a novel route for engineering spectrum linewidth. Combining BICs and polarization control facilitates a plethora of applications ranging from chiral molecule detection, valleytronics, and asymmetric photocatalysis to quantum information processing. As shown in Figure 3(a) and (b), a resonant metasurface consisting of tilted titanium dioxide (TiO_2) bar arrays and an indium tin oxide (ITO)-coated substrate is reported to produce highly efficient chiral emission with controllable spectra, radiation patterns, and spin angular momentum [109]. The structural symmetry of the meta-atom was broken by introducing an in-plane rotation angle and an out-of-plane tilted angle. A high Q-factor of 1250 and a high degree of

polarization of 98.9% were observed for the photoluminescence. The quasi-BIC of the resonant metasurface also supported ultracompact chiral lasing with a peak degree of polarization of 98.9%. Chen *et al.* [110] reported a slant-perturbation metasurface with intrinsic chiral BICs. The intrinsic chirality of the meta-atom broke both the in-plane and out-of-plane mirror symmetries by introducing an in-plane deformation angle and an out-of-plane slant angle. The local spin density variation could explain the slant meta-atom's optical chirality. A high circular dichroism (CD) of 0.93 and a high Q factor exceeding 2663 were experimentally verified at visible frequencies.

The CD and Q-factor for the chiral quasi-BIC resonances are generally related to each other. An increase in the asymmetric structures leads to a higher CD but is associated with an increased radiation loss and hence a lower Q-factor. Tang *et al.* recently reported a novel IRUE metasurface [111] that could independently control the CD and Q-factor by tuning the twist angle of the vertical split-ring resonator and the height of the wall, respectively (Figure 3(c)). The nonlocal surface lattice resonances caused the chiral quasi-BICs of the integrated resonance metasurface. The plasmonic metasurface showed a high Q-factor of 938 and a CD of 0.67 in the mid-infrared band. Liang *et al.* proposed a unique diatomic metasurface structure [112] that could achieve sharply different spectral responses for an arbitrary pair of orthogonal polarization states in full stocks, including linear, circular, and elliptical polarizations. The diatomic unit cell consisted of a vertically oriented split-ring resonator and a V-shaped meta-atom (Figure 3(d)), capable of independently controlling the absorption and mode polarization of the metasurface, respectively. Due to the near-field coupling between the dissimilar meta-atoms within the unit cell, the plasmonic metasurface produced an order of magnitude field enhancement compared to the canonical metal-dielectric-metal perfect absorbers.

The BIC can be utilized for enhancing not only linear chiroptical effects but also nonlinear responses. For example, a Si metasurface with broken-symmetry L-shaped meta-atoms (Figure 3(e)) was proposed to facilitate the generation of the third harmonic with a large nonlinear CD from +0.918±0.049 to −0.771±0.004 for different asymmetric structures [113]. Another example was the planar chiral metasurface [114] consisting of a square lattice of double-side scythe α-Si meta-atoms (Figure 3(f)). The BICs with strong birefringence of the planar chiral metasurface supported vortex elliptical eigen-polarizations with nonvanishing helicity. By breaking in-plane structure symmetry or tuning incident angles, maximal planar chirality could be achieved. A measured CD of 0.81 was attained for third-harmonic generation.

2. Amplitude and phase

The ability to manipulate the incident EM wave amplitude and phase simultaneously contributes to the hologram in the visible or near-IR band, as reported [24], [115], [116]. The holographic image can be reconstructed perfectly accord-
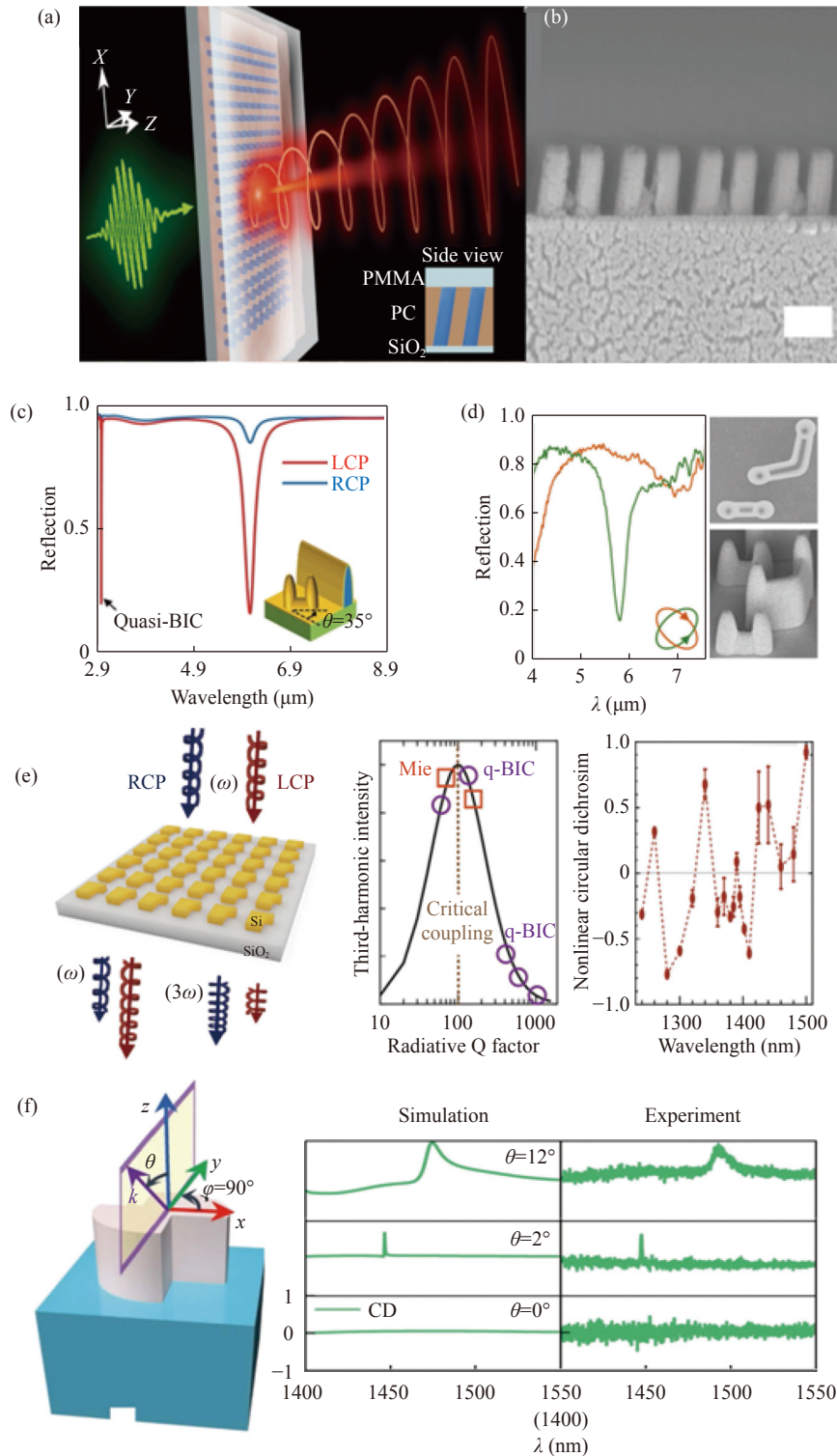
Figure 3 Simultaneous polarization and wavelength control. (a) Schematic of the metasurface for chiral emission [110]; (b) The corresponding SEM images of the fabricated metasurface's side-view; (c) The reflection spectra of the diatomic unit cell (inset) under the illuminations of two different circular polarizations [111]; (d) Top-view and oblique-view SEM images of the fabricated plasmonic diatomic metasurfaces and the measured reflection spectra [112]; (e) Schematic of the symmetry-broken silicon metasurface with L-shaped meta-atoms and its third-harmonic intensity and nonlinear CD [113]; (f) Schematic of the planar double-sided scythe α-Si meta-atom and its simulated and measured CD spectra for different incident angles [114].

ing to the targets, while the traditional images cannot. Additionally, the conventional hologram employs iterative algorithms, thus lowering the signal-to-noise ratio. The complex amplitude meta-hologram can be achieved in several

ways and significantly promote the advancement of holograms. Complex amplitude manipulation can be performed by expanding the Pancharatnam-Berry phase encoded onto the metasurface [115]. The PB phase is a geometric phase

achieved by the space-variant polarization manipulations. When two nanorods are combined as an X-shaped nanoantenna, the amplitude and phase can be independently modified by inducing an extra tuning component, as shown in Figure 4(d). The amplitude depends on the difference be-

tween the two nanorods' rotation angles, while the phase relies on their sum. According to the experimental results, the complex amplitude hologram shows an enhanced signal-to-noise ratio over the traditional holograms, which usually lose amplitude information.
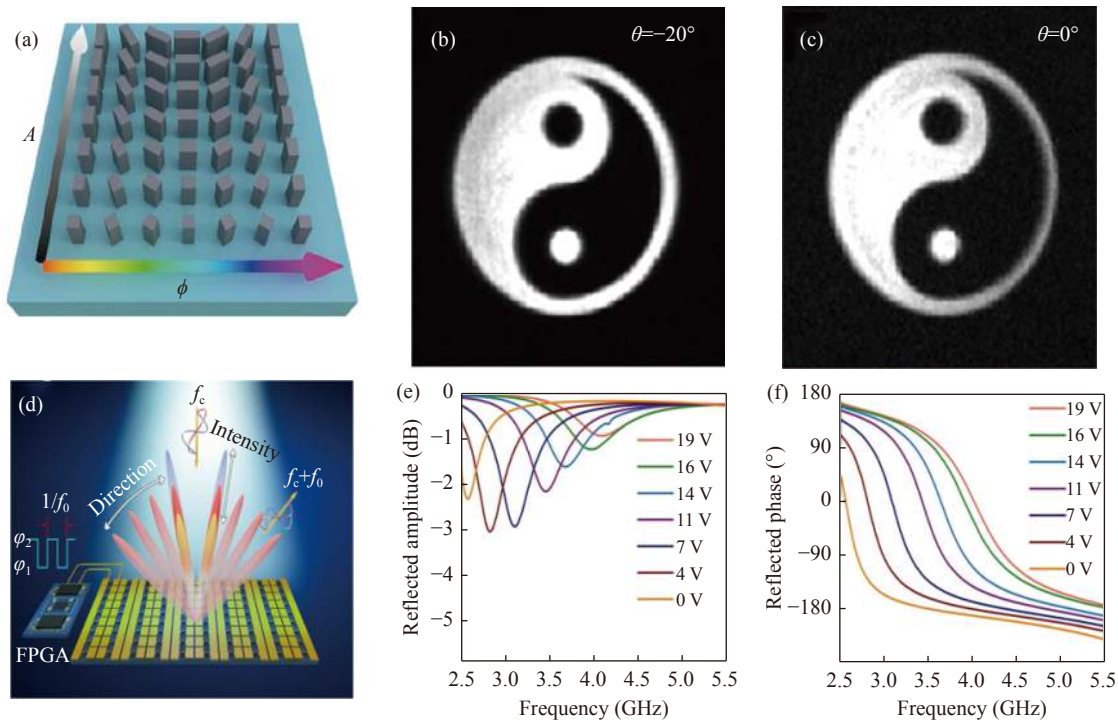
Figure 4 Complex amplitude manipulation of the light field. (a)–(c) Dimensions and orientations of the unit cells to independently modulate the amplitude and phase (a), reconstructed holographic images at an observation angle of −20 degrees (b), and the reconstructed holographic images at an observation angle of 0 degrees (c) [116]. (d)–(e) Schematic of the harmonic amplitudes and phases control (d), amplitude (e), and phase (f) spectra under different bias voltages [117].

The modulation mechanism is acheived by varying the size and rotation angle of a single nanoantenna (Figure 4(a)) [116]. Altering the orientation of the adjustable size X-shaped nanoantenna is another expansion of the geometry phase principle. The phase varies with respect to the rotation angle of the nanoantenna, while the amplitude is modulated by varying the birefringence, which determines the circular polarization conversion rate and thus defines the transmitted amplitude. This ability is demonstrated by designing two holograms with the same amplitude but different phases. The holographic images can be observed from different angles by patterning the two holograms with different gradient phases (Figure 4(b) and (c)). A 3D coil is also reconstructed to show the superiority of the design method.

Apart from varying the horizontal dimensions, altering the height of the nanopillar can also tune the transmitted amplitude. Combined with the rotation angle, the joint regulation of amplitude and phase can be accomplished [24]. The regulation method can be implemented with the help of three-dimensional printing technology, i.e., two-photon polymerization. Two-photon direct writing is a precise 3D micro/nanofabrication technique for creating microstructures and photonic devices using high-power laser

beams to etch or polymerize materials. It differs from traditional single-photon lithography by using two laser beams to achieve high resolution and sensitivity, restricting photoreactions to the focal point [118]. With the use of this method, Maier *et al.* demonstrated an OAM multiplexing meta-hologram [24]. Up to two hundred holographic images were encoded into a single metasurface. Every two images were related to one OAM state and was reconstructed in different planes. The crosstalk was suppressed due to the joint manipulation of amplitude and phase, and the reconstructon of two holographic videos in a single meta-hologram was attainable.

Another important application that is relevant to everyone and requires precise control of amplitudes and phases is wireless communication. Mobile communications always need harmonic manipulation. To customize the harmonics, a commonly used method involves incorporating supplementary amplifiers and phase shifters to meticulously regulate the amplitudes and phases of the harmonics after the mixing process. However, this approach is known to cause costly expenditures and system integration challenges. Cui *et al.* demonstrated a 1-bit time-domain digital coding metasurface scheme to achieve the required harmonic control (Figure 4(d), (e) and (f)) [117]. The harmonic amplitudes

were modulated by the phase differences of the two states defined by the biased voltages. The phase distribution of the harmonics was subject to the time delay of the switching functions for the meta-atoms.

The ability to control the amplitude and the phase simultaneously strengthens the metasurface to completely handle the wavefront of the EM waves and performs various advanced functions from holograms to wireless communications [119]–[124].

3. Polarization and phase

EM waves have vectoriality. Therefore, incorporating polarization control into the functionality of metasurfaces, mostly phase modulation, can cause them to be more versatile and meet the requirements in a more comprehensive range of applications [125]–[133].

For example, a metalens can work in a virtual imaging device. It usually has a single focal spot defined by the focusing phase profile encoded onto the metasurface. The most immediate change observed is the multiple focal spots once inducing the DOF of polarization [134]. Multifocal metalenses can focus incoming light on multiple focal points, enabling the simultaneous capture of multidimensional information. Yang *et al.* developed an imaging system including a single mete-lens with two focus spots and the corresponding image retrieval algorithm to obtain the depth and polarization information within a single shot [135]. They were well suited for applications requiring variable focal lengths, such as zooming in and out, making them ideal for video cameras, telescopes, and microscopes [136].

Additionally, due to the polarization-selective multifocal metalens, various advanced imaging applications are more easily performed, including chiral imaging. Usually, polarization imaging is performed using cascading multiple lenses and waveplates. A much more compact way is to combine the lenses and the waveplates into a single metasurface (Figure 5(a)) [137]. A chiral beetle can be observed under opposite helicity, showing diverse information by focusing the opposite circular polarization components from the imaging target into different spots (Figure 5(b)). The multiple-focus meta-lens faciliates a very intuitive, elegant, and simple avenue to perform polarization imaging.

The vectoriality of EM waves contributes to vectorial meta-holograms for various fancy functions and applications. For example, Li *et al.* proposed a metasurface design scheme for independently controlling the phase and polarization and demonstrated holographic image reconstruction with arbitrarily spatially varying polarization states (Figure 5(c)) [138]. The supercell of the proposed diatomic metasurface consisted of two silver nanorods. These two nanorods were always perpendicular to each other. Thus, the reflected light could be observed as the composition of the two orthogonal field components modulated by the two nanorods in the supercell. The whole supercell defined the phase. Moreover, the polarization state could be tuned by varying the amplitude and phase differences of the field modulated by the two nanorods. Specifically, the phase dif-

ference between these two components depended on the relative position displacement; the rotation angles of the nanorods determined the amplitude ratio. Note that the two nanorods were always set as orthogonal. In this way, the phase and polarization could be tuned independently; the encoding of the holographic image and the polarization state at the subwavelength level was attainable. The diatomic design made it much simpler to simultaneously modulate phase and polarization parameters. Moreover, this approach effectively mitigated the challenges associated with the design and fabrication processes by maintaining the same size and shape of meta-atoms.

Another scheme to utilize the polarization channel in holograms is to perform encryption. The encrypted information can be allocated into the opposite circular polarization components. Li *et al.* demonstrated a multiplexing vectorial meta-hologram [139]. Twin holographic images were encoded into the two circular polarization channels. Additional information could be encrypted using the overlap area (Figure 5(d)). The image in the overlapped area could be dynamic by continuously altering the phase difference between the incident right and left circularly polarized light. This dual-function device improved communication security by providing the twin images. The designed IRUE could be used to independently control phase profiles of the orthogonal polarization components and compensate for the broadband phase by integrating the propagation phase and geometric phase (Figure 5(e)) [44], [140]. The polarization-dependent holograms are shown (Figure 5(f)).

4. Wavelength and phase

Metasurfaces for frequency manipulation can be divided into two types, i.e., nonlinear metasurfaces [141]–[145] and temporally modulated metasurfaces [146], [147], each of which has advantages and limitations. Nonlinear metasurfaces can significantly enhance the nonlinear response of natural materials due to the strong resonant field enhancement. Furthermore, nonlinear metasurfaces are free of stringent phase-matching requirements since the nonlinear process only occurs in a subwavelength-thick layer. However, the nonlinear process requires high optical pump power, and the overall frequency efficiency still needs improvement; currently, plasmonic structures achieve an efficiency of $\sim 10^{-10}$ [141]–[143] and all-dielectric designs achieve an efficiency of $\sim 10^{-6}$ [144], [145]. On the other hand, temporally modulated metasurfaces leverage the time domain as another degree of freedom for light manipulation, enabling regulation of the frequency property of EM waves. Temporally modulated metasurfaces can achieve a theoretical maximum frequency-conversion efficiency of 100% for serrodyne modulation with saw tooth phase modulation [146], [147]. However, temporally modulated metasurfaces typically have a slight frequency shift of light from the kHz to GHz range. Most temporally modulated metasurfaces are experimentally demonstrated at microwave frequencies due to the available mature active control components, such as varactor diodes and PIN diodes, as well as printed circuit
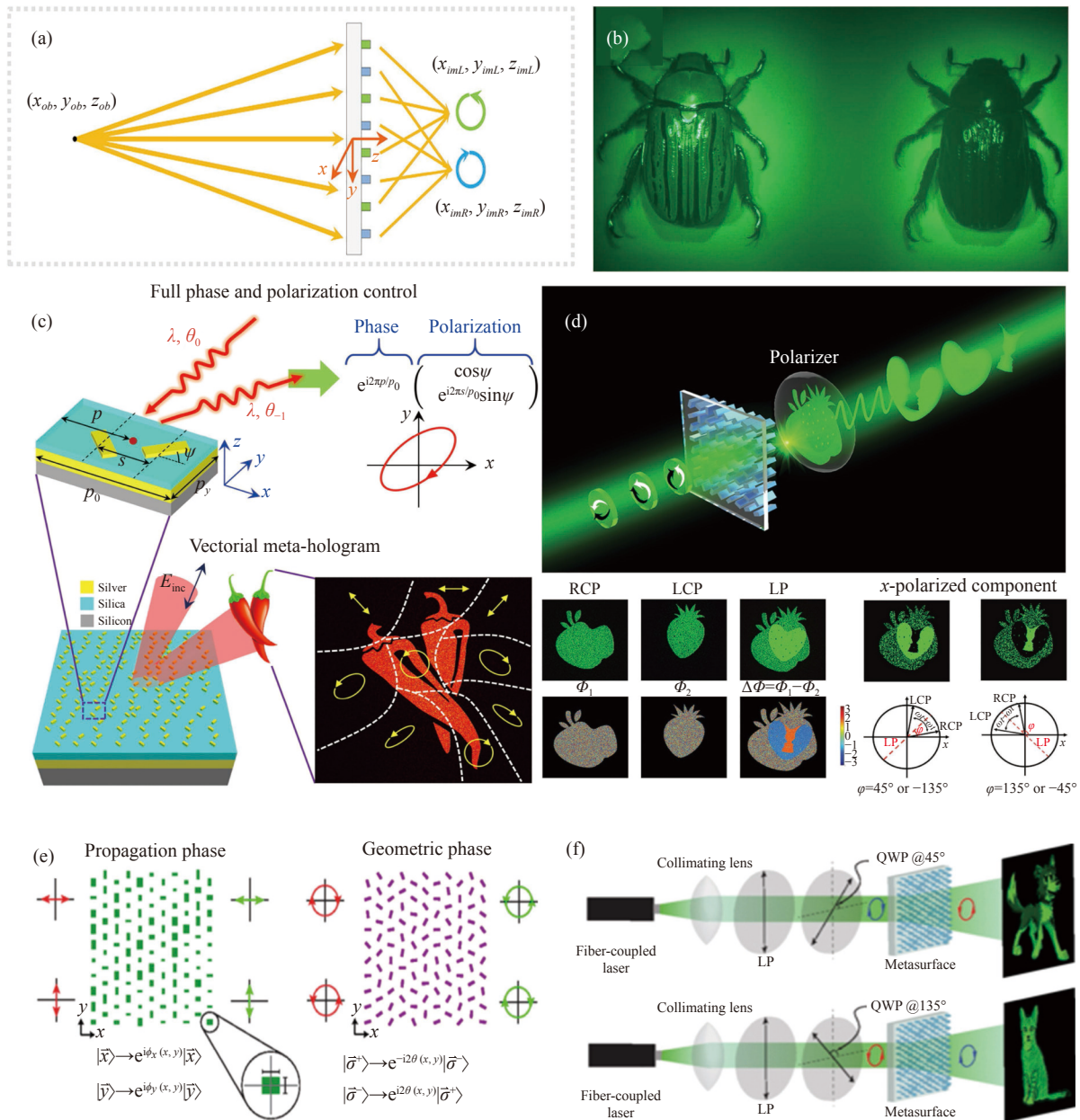
Figure 5 Polarization and phase manipulation of the light field. (a) Circular polarization multiplexed metalens [137]; Different focal points for LCP and RCP components allow viewing of an object through images from both. (b) Images shown at the two focuses for the LCP and RCP light. (c) Diatomic metasurface for vectorial holography [138]; The phase difference depends on the relative position displacement, and the amplitude ratio depends on the rotation angles of nanorods. (d) Overlap region hologram for encryption [139]. (e) IRUE design for vectorial applications [140]; The IRUE design can control the phase profiles of arbitrary orthogonal polarization components using propagation and geometric phases. (f) Vectorial hologram reconstructed by the IRUE-designed metasurface [140].

board (PCB) technologies.

Temporally modulated metasurfaces incorporating spatial modulation, namely, spatiotemporally modulated metasurfaces, have attracted extensive attention due to their appealing flexibility for controlling the frequency and phase properties of light [8], [148]–[151]. Applying time-gradient control signals to the meta-atoms results in an equivalent phase gradient at one specific harmonic, thereby steering the beam in the intended direction [148]. Nevertheless, spatiotemporally modulated metasurfaces generally produce undesired harmonics (sideband), reducing the frequency

conversion efficiency and polluting useful signals. This limitation has been recently overcome by integrating a spatiotemporally modulated metasurface with a waveguide, namely, space-time-coding (STC) metasurface antennas [8], [152], [153], as shown in Figure 6(a). The STC metasurface antenna can translate the in-plane guided waves into out-of-plane propagating waves with a desired converted frequency in free space. Due to the enormous momentum mismatch, the undesired harmonics are suppressed in both free space and the waveguide. A high frequency-conversion efficiency of ~80% and beam steering have been demon-

strated for space-time-coding metasurface antennas through 1-bit ON-OFF switching of the coupling state of the meta-atoms. The STC metasurface antenna can simultaneously generate and independently manipulate multiple harmonics and their wavefronts by sharing the same radiating aperture (Figure 6(b)).

Nonlinear metasurfaces significantly enhance the nonlinear response of natural materials and provide the flexibility to efficiently engineer the phase of nonlinear waves. Phase control for nonlinear metasurfaces can be implemented by a geometric PB phase for circular polarization (CP) or

an abrupt phase change for linear polarization incidence. The introduced geometric PB phases for nonlinear waves are $(n-1)\theta\sigma$ and $(n+1)\theta\sigma$ for different circular polarization nonlinear waves [156]. $\sigma = \pm 1$ and represents for the same or opposite circular polarizations to that of the fundamental wave, n is the nonlinear order, and θ is the orientation angle of the meta-atom. Furthermore, only a particular harmonic order with a specific circular polarization can be generated by carefully designing the rotational symmetry of the meta-atom [156]. For example, Tseng et al. demonstrated a nonlinear metalens that simultaneously achieved sec-
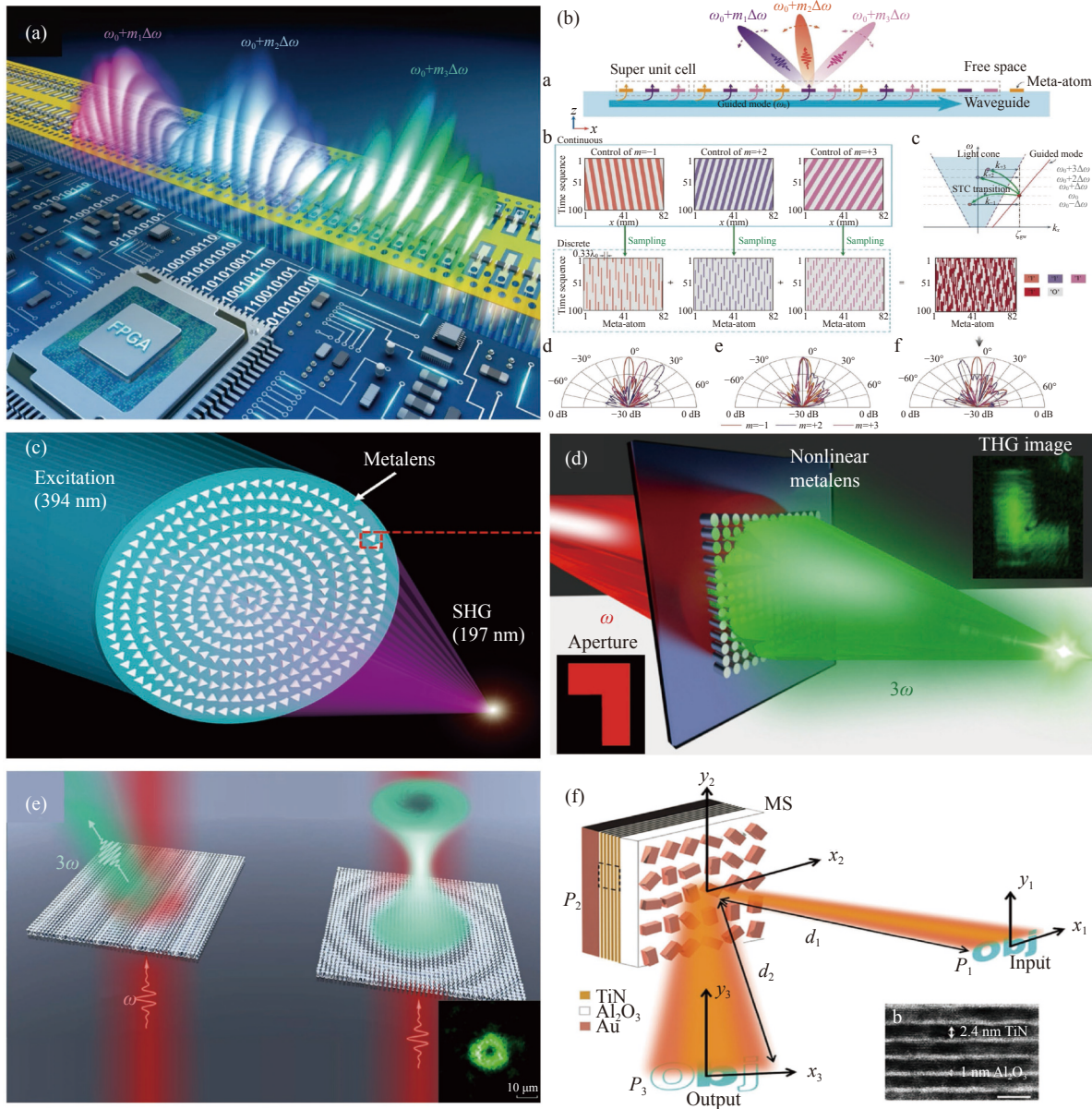
Figure 6 Simultaneous wavelength and phase control. (a)–(b) Illustration of the space-time modulated metasurface antenna and (a) experimental demonstration of multiharmonic independent control (b) [8]. (c) Concept illustration of the nonlinear dielectric metasurface with triangular-shaped ZnO meta-atoms for generating focused second-harmonic vacuum ultraviolet light [154]. (d) Third-harmonic generation and focusing of the fundamental Gaussian beam by the nonlinear dielectric metalens. (e) Concept illustration of the nonlinear dielectric metasurface for third-harmonic beam deflection (left) and third-harmonic vortex beam generation (right) [145]. The bottom right inset shows the measured field intensity of a donut-shaped vortex beam at the third-harmonic frequency. (f) Conceptual illustration of the nonlinear computational imaging metalens for image edge detection [155]. The bottom right inset shows a transmission electron microscope image of the metallic quantum wells.

ond-harmonic generation and light focusing at vacuum ultraviolet frequencies [154]. A triangularly shaped zinc oxide (ZnO) meta-atom with C_3 rotational symmetry (Figure 6(c)) was adopted to achieve a full 2π phase range for the nonlinear wave by rotating the meta-atom. The nonlinear metalens could convert the 394 nm fundamental light into focused 197 nm radiation with a 1.7 µm-diameter spot.

Elliptical nanopillar Si-based meta-atoms with different geometric dimensions are used for linearly polarized pump waves to provide a full 2π phase range for the third-harmonic field. The electric and magnetic Mie resonances facilitate nonlinear efficiency enhancement and high directionality of the nonlinear waves. Different wavefront shaping, including beam deflection, vortex beam generation, and light focusing [145], is demonstrated for the all-dielectric nonlinear metasurface at the third-harmonic frequency, as shown in Figures 6(d) and (e). Nonlinear metasurfaces with simultaneous frequency conversion and wavefront engineering provide a new route to many applications. One illustrative example is computational edge detection [155], as shown in Figure 6(f). By using metallic quantum wells with intensity-dependent optical constants, the phase difference of the two sheared images can be tuned by the input intensity. Therefore, a single nonlinear metasurface can achieve different computational imaging from an edge image to a diffracted full image by tuning the illumination light intensity.

5. Polarization, amplitude, and phase

With further increased DOFs of the EM wave tailored by metasurfaces, much more versatile and promising high-dimensional light field manipulation functions can be achieved by tailoring the complex amplitude of both orthogonal polarization channels.

For example, the information can be encoded into the metasurface as a hologram in the far field and nanoprinting in the near field in multiple polarization channels. The first experimental single-layer metasurface demonstration of encoding four independent channels of optical information, two holograms, and two nanoprinting images in orthogonal polarization states was shown by Xu *et al.* [157]. The birefringent elements were selected as the nanoantennas, and thus, the orthogonal polarizations had opposite-handedness after being modulated by the nanoantenna. Thus, the Jones matrix solved the complex amplitude modulation in both polarization channels. They found that the Jones matrix of the unit cell for the control of the complex amplitude of both channels could be expressed as a combination of two different Jones matrices. This solution was intuitive and easily applied to practice. The unit cell was composed of two birefringent elements, and each was responsible for one of the Jones matrices by varying the dimensions and the orientations. As a demonstration, they encoded dual holographic images and dual nanoprinting images in both circular polarizations (Figure 7(a)) [140]. Figure 7(b) shows the two nanoprinted images and the holographic images encoded in the single-layer metasurface. The proposed intuitive

design method and the demonstrated platform provide possibilities of concurrent and autonomous manipulation of both the phase and amplitude for two orthogonal polarizations. In addition, this design can function across a broad range of frequencies, enabling the reconstruction of full-color images using both nanoprinting and holographic techniques.

Thus, the Jones matrix method has been proven to be a practical approach for addressing wavefront transformation issues related to polarization. This method was soon expanded to increase the information channels, i.e., triple sets of nanoprinting and holographic images encoded in a single-layer metasurface (Figure 7(c)) [158]. The unit cell of the proposed metasurface was composed of four nanoblocks of the exact same dimensions with different orientations. The nanoantenna was optimized to only respond to the polarization parallel to its long axis. The output Jones matrix could be expressed as six equations for an arbitrary incident polarization. As three pairs of amplitudes and phases needed to be determined, a unit cell required at least three nanoantennas providing six DOFs (three pairs of positions and orientations). An additional nanoantenna was included in the unit cell to prevent potential overlap, referring to the upper right corner of Figure 7(c). The bottom panel of Figure 7(c) shows the experimental results of the triple groups of encoded images, the nonprinted faces, and the reconstructed letters.

Polarization-controlled wavefront manipulation can also contribute to the dynamic optical display (Figure 7(d)) [159]. This is achieved by tailing the polarization distributions in addition to the complex amplitude distribution, and the polarization does not work as an information channel. This technology enables the invention of elaborate and appealing visual displays that can be used in various scenes, from entertainment to scientific research.

Integrating the polarization dimension into complex amplitude wavefront modulation provides numerous advantages in various applications [160], from enhancing the information capacity to dynamic display and polarized space folding.

6. Polarization, wavelength, and phase

Broadband and narrowband wavefront shaping both have significance in related areas. Broadband modulation is essential for full-color display applications. In contrast, spectral control is sometimes necessary, especially when only part of the wavelengths need polarization and phase modulation, leaving others unaffected.

The quasi-BIC has emerged as an effective spectral control method, including spectral polarization and phase control. Alù *et al.* proposed a metasurface supporting chiral BICs. The unit cell of the metasurface was composed of two sets of stacked nanopillars with different twist angles (inset of left panel, Figure 8(a)). This could achieve strong chiral effects in a selected narrowband. Combined with the PB phase principle, the metasurface could tailor the phase of the selected spectral of the incident beam while leaving
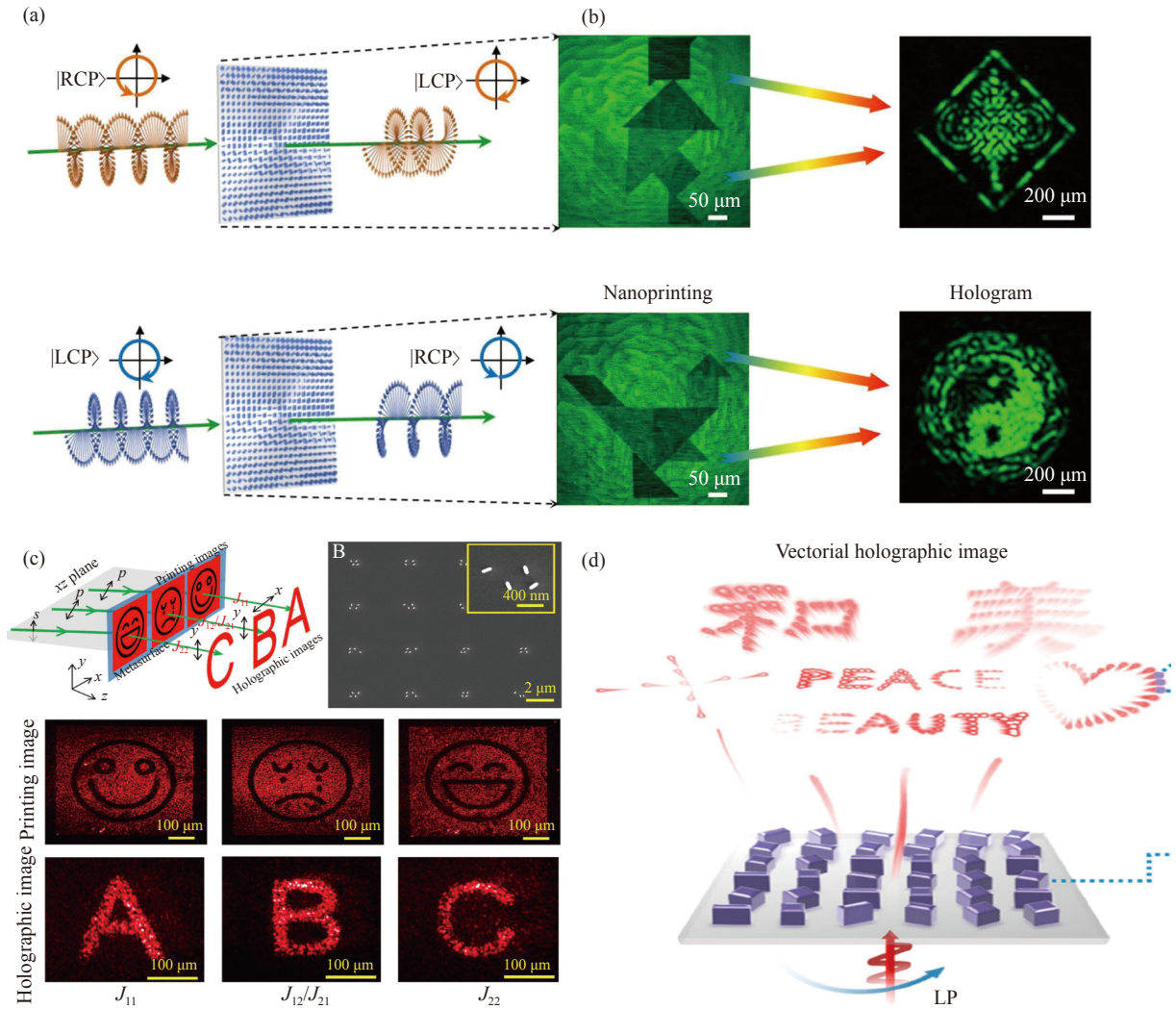
Figure 7 Polarization, amplitude, and phase manipulation of the light field. (a) Single-layer multifunctional metasurface for independent and arbitrary amplitude and phase control for orthogonal polarization states [140]; (b) Experimental results of two nanoprinting images and the holographic images encoded in the single-layer metasurface [140]; (c) Design and experimental result of the triplet set of nanoprinted hologram images [158]; (d) Dynamic vectorial holography [159]; The input beam is linearly polarized, and the output field can be dynamically modulated using a polarizer and analyzer to create spatially varying polarizations and intensities.

others transmitting without modulation (left of Figure 8(a)). The right panel of Figure 8(a) shows the simulated tilted plane wave under gradient phase modulation. Figure 8(b) shows the mode distribution under resonance excitation incidence. Figure 8(c) displays the far fields under different circular polarizations, and the near-unity anomalous reflection can only be excited under right circular polarization. The proposed design method could be used to perform more complex wavefront tailoring, especially when there is a requirement to encode different phase profiles to specific wavelengths [161].

The complete phase and polarization manipulation enable the vectorial hologram of continuous vector variation, leading to better information encoding. However, color, which is one of the most intuitive features for human beings to understand the world, has not yet considered. To fully use such properties, Zhao *et al.* demonstrated a full-color and arbitrary polarization hologram (Figure 8(d)) [162]. For

the first time, they showed a minimalist and exquisite design method to fully tune the polarization and color of the incident beam. The unit cell was composed of two kinds of rectangular nanoantennas. Under linear polarization incidence, these two nanoantennas generated two circular polarization states in their ±1 (or opposite) diffraction orders (Figure 8(e)). The output of a single unit cell was the sum of the two components; thus, the variation of its phase and amplitude by tuning the orientations of the two kinds of nanoantennas was possible, and the polarization states were defined. As polarization control was attained in the first diffraction order, it could perform full color holography with arbitrary polarizations through k-space ptychography [165]. When selecting the dimensions of the nanoantennas, the holographic images will be reconstructed with the same polarization states only if the phase compensation of the three primary colors (633 nm, 532 nm, and 473 nm) is fulfilled. The proposed minimalist approach effectively cir-
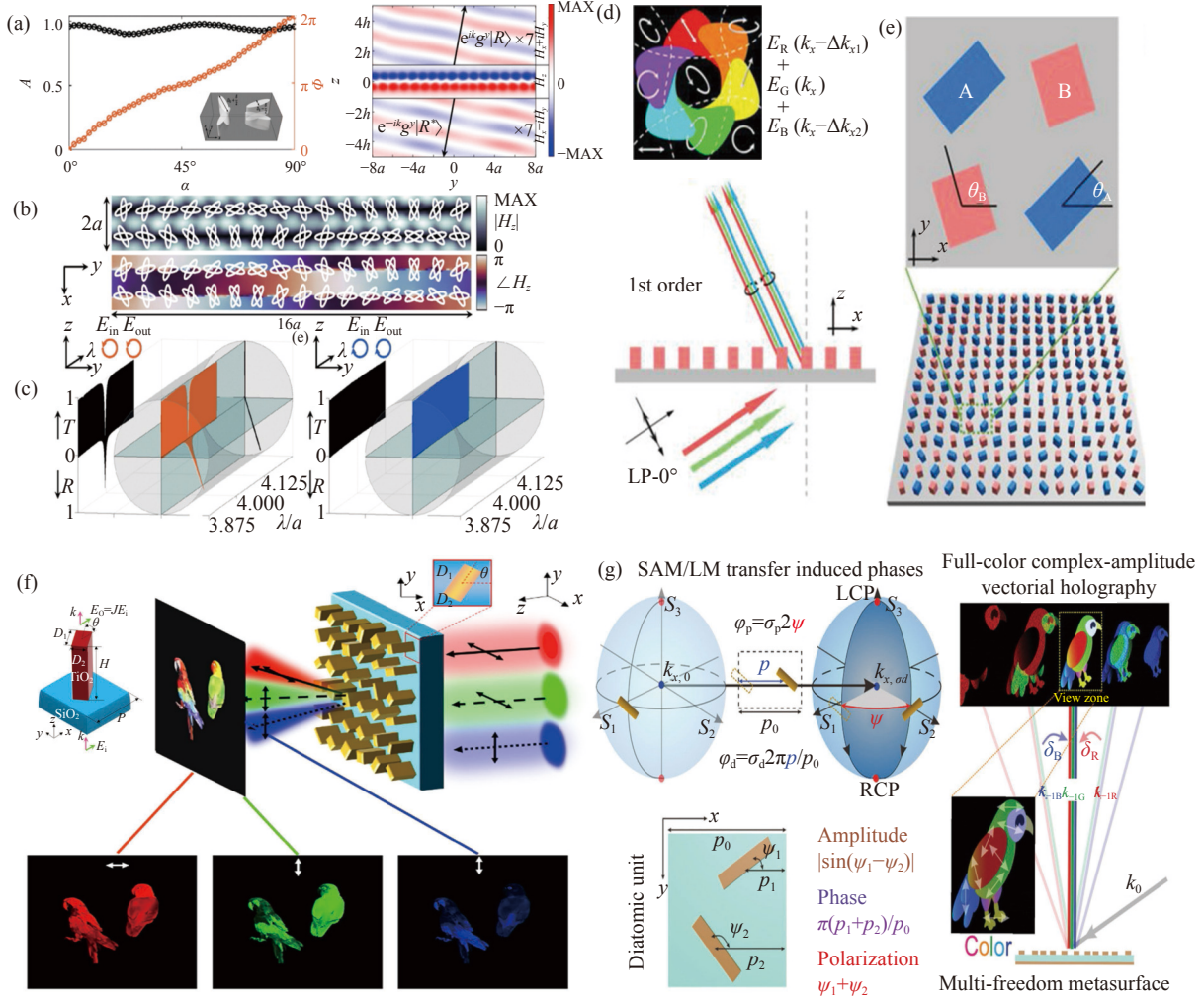
Figure 8 Polarization wavelength and phase manipulation of the light field. (a)–(c) Chiral quasi-bound states in the continuum [162]: (a) Chiral BIC metasurface for phase control [162]; (b) Mode distribution under resonance excitation incidence; (c) Far fields under different circular polarizations. (d) Schematic of the full-color and arbitrary polarization hologram [163]. (e) Unit cell design of the tetratomic metasurface. (f) Trichromatic and tri-polarization-channel holography [164]. (g) Method of full-color complex-amplitude vectorial holograms.

cumvented the need for complex nanostructure searching and challenging fabrication processes.

Duan *et al.* demonstrated a full-color hologram by integrating multiple polarization channels [164]. Three primary colors and three polarization channels were multiplexed using a noninterleaved metasurface (Figure 8(f)). The advantage was that the crosstalk was almost zero, and there was no interleaving-induced degradation of efficiency; thus, the reconstructed holographic images had high quality. Their work was the first demonstration of a full-color hologram with near-zero crosstalk.

The co-manipulation of the DOFs of polarization, wavelength, and phase shows the potential of advanced wavefront manipulation. For example, various advanced holograms have been demonstrated. Li *et al.* further perfected EM wave manipulation by integrating the DOF of amplitude [166]. They first derived analytical equations from seamlessly tailoring the phase, polarization, and amplitude achieved by the geometric and detour phases unrelated to wavelengths. The wavelength multiplexing was then inte-

grated using the k-space engineering technique to reconstruct a full-color complex-amplitude vectorial meta-hologram (Figure 8(g)).

Multidimensional manipulation of light is a groundbreaking capability that opens up new possibilities for producing novel phenomena and facilitating various applications, including the precise and reliable reconstruction of the optical information.

IV. Conclusion and Perspectives

We have reviewed the research progress of metasurfaces in recent years from the perspective of different EM wave modulation dimensions. Single-dimensional modulation includes phase, polarization, amplitude, wavelength, and orbital angular momentum. Multidimensional modulations include polarization-wavelength modulation, amplitude-phase modulation, polarization-phase modulation, wavelength-phase modulation, polarization-amplitude-phase modulation, polarization-wavelength-phase modulation, and polarization-wavelength-phase-amplitude modulation. The performance

of single-dimensional modulation is limited in specific scenarios. However, after multidimensional modulation, the limitations of single-dimensional modulation can be overcome, and more flexible and diverse EM properties can be obtained. The advantages consist of achieving multiplex-oriented applications, such as massive information storage, transmission, and exotic vectorial field reconstructions. It has broad application prospects for the full potential of advanced EM field manipulation.

We anticipate several promising avenues for high-dimensional control of EM waves, which have the potential to exert a profound impact on EM devices.

Development of multidimensional applications Multidimensional modulation primarily focuses on two dimensions, with demonstrated applications mainly in holography and nanoprinting. Therefore, two important research directions are to increase the modulation dimensions and to explore new applications.

Achieving independent manipulation of every dimension of electromagnetic waves is challenging because the dimensions are intrinsically linked when varying the meta-atoms' geometrical parameters. Therefore, the determination of a method to decouple the links is highly important.

Metasurfaces have numerous advantages over conventional devices, making them a promising direction to develop new applications using well-established high-dimensional modulation principles. By leveraging these advantages and exploring new applications, metasurfaces could facilitate new possibilities for manipulating light and advancing optical technologies.

Development of multidimensional and tunable meta-devices The functionalities of multidimensional modulation devices are predominantly static. Nevertheless, practical demands necessitate flexible and adaptable control. For instance, in the field of holography, existing multidimensional modulation devices are typically limited to producing holograms with fixed patterns. However, in practical applications, such as 3D displays or security systems, the dynamic and flexible manipulation of EM wavefronts is crucial for achieving optimal performance and functionality. Therefore, there is a need to develop tunable devices under high-dimensional modulation that can provide flexible and adaptable control over EM waves.

Integrating multidimensional modulation devices into a practical system While many significant advancements have been made in the research and functional demonstration of electromagnetic wave control principles, their practical applications in engineering are still limited. Despite the successes, many challenges need to be overcome to achieve practical implementation, such as the development of highly efficient and cost-effective technologies that can operate effectively in the real-world environment. Hence, further efforts are needed to bridge the gap between theoretical research and practical engineering applications [167]–[169] and to identify new solutions that can meet the demands of industry and society.

References

[1] L. Zhou, L. Tsang, V. Jandhyala, *et al*., "Emissivity simulations in passive microwave remote sensing with 3-D numerical solutions of maxwell equations," *IEEE Transactions on Geoscience and Remote Sensing*, vol. 42, no. 8, pp. 1739–1748, 2004.

[2] L. Li, J. Vivekanandan, C. H. Chan, *et al*., "Microwave radiometric technique to retrieve vapor, liquid and ice. I. Development of a neural network-based inversion method," *IEEE Transactions on Geoscience and Remote Sensing*, vol. 35, no. 2, pp. 224–236, 1997.

[3] Y. X. Cao, S. Yan, W. D. Liu, *et al*., "A wideband multibeam pill-box antenna based on differentially fed leaky-wave array," *IEEE Antennas and Wireless Propagation Letters*, vol. 22, no. 3, pp. 512–516, 2023.

[4] G. B. Wu, K. F. Chan, and C. H. Chan, "3-D printed terahertz lens to generate higher order bessel beams carrying OAM," *IEEE Transactions on Antennas and Propagation*, vol. 69, no. 6, pp. 3399–3408, 2021.

[5] H. Yi, S. W. Qu, K. B. Ng, *et al*., "3-D printed millimeter-wave and terahertz lenses with fixed and frequency scanned beam," *IEEE Transactions on Antennas and Propagation*, vol. 64, no. 2, pp. 442–449, 2016.

[6] Q. L. Zhang, B. J. Chen, K. F. Chan, *et al*., "Terahertz circularly- and linearly polarized leaky-wave antennas based on spin-orbit interaction of spoof surface plasmon polaritons," *IEEE Transactions on Antennas and Propagation*, vol. 69, no. 8, pp. 4347–4358, 2021.

[7] R. S. Aspden, N. R. Gemmell, P. A. Morris, *et al*., "Photon-sparse microscopy: Visible light imaging using infrared illumination," *Optica*, vol. 2, no. 12, pp. 1049–1052, 2015.

[8] G. B. Wu, J. Y. Dai, Q. Cheng, *et al*., "Sideband-free space-time-coding metasurface antennas," *Nature Electronics*, vol. 5, no. 11, pp. 808–819, 2022.

[9] J. C. Zhang, G. B. Wu, M. K. Chen, *et al*., "A 6G meta-device for 3D varifocal," *Science Advances*, vol. 9, no. 4, article no. eadf8478, 2023.

[10] Q. Ma, C. Liu, Q. Xiao, *et al*., "Information metasurfaces and intelligent metasurfaces," *Photonics Insights*, vol. 1, no. 1, article no. R01, 2022.

[11] S. J. Ma, B. Yang, and S. Zhang, "Topological photonics in meta-materials," *Photonics Insights*, vol. 1, no. 1, article no. R02, 2022.

[12] Y. H. Guo, M. B. Pu, F. Zhang, *et al*., "Classical and generalized geometric phase in electromagnetic metasurfaces," *Photonics Insights*, vol. 1, no. 1, article no. R03, 2022.

[13] A. S. Solntsev, G. S. Agarwal, and Y. S. Kivshar, "Metasurfaces for quantum photonics," *Nature Photonics*, vol. 15, no. 5, pp. 327–336, 2021.

[14] M. K. Chen, X. Y. Liu, Y. N. Sun, *et al*., "Artificial intelligence in meta-optics," *Chemical Reviews*, vol. 122, no. 19, pp. 15356–15413, 2022.

[15] P. C. Wu, W. T. Chen, K. Y. Yang, *et al*., "Magnetic plasmon induced transparency in three-dimensional metamolecules," *Nanophotonics*, vol. 1, no. 2, pp. 131–138, 2012.

[16] M. Semmlinger, M. L. Tseng, J. Yang, *et al*., "Vacuum ultraviolet light-generating metasurface," *Nano Letters*, vol. 18, no. 9, pp. 5738–5743, 2018.

[17] N. F. Yu, P. Genevet, M. A. Kats, *et al*., "Light propagation with phase discontinuities: Generalized laws of reflection and refraction," *Science*, vol. 334, no. 6054, pp. 333–337, 2011.

[18] S. L. Sun, Q. He, S. Y. Xiao, *et al*., "Gradient-index meta-surfaces as a bridge linking propagating waves and surface waves," *Nature Materials*, vol. 11, no. 5, pp. 426–431, 2012.

[19] S. L. Sun, K. Y. Yang, C. M. Wang, *et al*., "High-efficiency broadband anomalous reflection by gradient meta-surfaces," *Nano Letters*, vol. 12, no. 12, pp. 6223–6229, 2012.

[20] N. Shitrit, I. Bretner, Y. Gorodetski, *et al*., "Optical spin hall effects in plasmonic chains," *Nano Letters*, vol. 11, no. 5, pp. 2038–2042, 2011.

[21] V. C. Su, C. H. Chu, G. Sun, *et al*., "Advances in optical metasurfaces: Fabrication and applications [invited]," *Optics Express*, vol. 26, no. 10, pp. 13148–13182, 2018.

[22] Y. B. Fan, P. Tonkaev, Y. H. Wang, *et al*., "Enhanced multiphoton processes in perovskite metasurfaces," *Nano Letters*, vol. 21, no. 17, pp. 7191–7197, 2021.

[23] Y. B. Fan, Y. H. Wang, N. Zhang, *et al*., "Resonance-enhanced three-photon luminesce via lead halide perovskite metasurfaces for optical encoding," *Nature Communications*, vol. 10, no. 1, article no. 2085, 2019.

[24] H. R. Ren, X. Y. Fang, J. Jang, *et al*., "Complex-amplitude metasurface-based orbital angular momentum holography in momentum space," *Nature Nanotechnology*, vol. 15, no. 11, pp. 948–955, 2020.

[25] G. B. Wu, Y. S. Zeng, K. F. Chan, *et al*., "3-D printed 3-D near-field focus-scanning lens for terahertz applications," *IEEE Transactions on Antennas and Propagation*, vol. 70, no. 11, pp. 10007–10016, 2022.

[26] G. B. Wu, K. F. Chan, K. M. Shum, *et al*., "Millimeter-wave and terahertz OAM discrete-lens antennas for 5G and beyond," *IEEE Communications Magazine*, vol. 60, no. 1, pp. 34–39, 2022.

[27] Y. X. Cao, S. Yan, S. F. Wu, *et al*., "3D printed multi-beam OAM antenna based on quasi-optical beamforming network," *Journal of Lightwave Technology*, vol. 41, no. 7, pp. 2196–2204, 2023.

[28] Y. H. Wang, Y. B. Fan, X. D. Zhang, *et al*., "Highly controllable etchless perovskite microlasers based on bound states in the continuum," *ACS Nano*, vol. 15, no. 4, pp. 7386–7391, 2021.

[29] C. H. Chu, M. L. Tseng, J. Chen, *et al*., "Active dielectric metasurface based on phase-change medium," *Laser & Photonics Reviews*, vol. 10, no. 6, pp. 986–994, 2016.

[30] T. J. Cui, M. Q. Qi, X. Wan, *et al*., "Coding metamaterials, digital metamaterials and programmable metamaterials," *Light: Science & Applications*, vol. 3, no. 10, article no. e218, 2014.

[31] J. Yao, R. Lin, M. K. Chen, *et al*., "Integrated-resonant metadevices: A review," *Advanced Photonics*, vol. 5, no. 2, article no. 024001, 2023.

[32] D. Sievenpiper, L. J. Zhang, R. F. J. Broas, *et al*., "High-impedance electromagnetic surfaces with a forbidden frequency band," *IEEE Transactions on Microwave Theory and Techniques*, vol. 47, no. 11, pp. 2059–2074, 1999.

[33] L. Zhou, W. Wen, C. T. Chan, *et al*., "Electromagnetic-wave tunneling through negative-permittivity media with high magnetic fields," *Physical Review Letters*, vol. 94, no. 24, article no. 243905, 2005.

[34] J. M. Hao, Y. Yuan, L. X. Ran, *et al*., "Manipulating electromagnetic wave polarizations by anisotropic metamaterials," *Physical Review Letters*, vol. 99, no. 6, article no. 063908, 2007.

[35] C. Qu, S. J. Ma, J. M. Hao, *et al*., "Tailor the functionalities of metasurfaces based on a complete phase diagram," *Physical Review Letters*, vol. 115, no. 23, article no. 235503, 2015.

[36] S. L. Sun, Q. He, J. M. Hao, *et al*., "Electromagnetic metasurfaces: Physics and applications," *Advances in Optics and Photonics*, vol. 11, no. 2, pp. 380–479, 2019.

[37] N. L. Mou, X. L. Liu, T. Wei, *et al*., "Large-scale, low-cost, broadband and tunable perfect optical absorber based on phase-change material," *Nanoscale*, vol. 12, no. 9, pp. 5374–5379, 2020.

[38] M. Khorasaninejad and F. Capasso, "Metalenses: Versatile multifunctional photonic components," *Science*, vol. 358, no. 6367, article no. eaam8100, 2017.

[39] X. Y. Liu, M. K. Chen, C. H. Chu, *et al*., "Underwater binocular meta-lens," *ACS Photonics*, vol. 10, no. 7, pp. 2382–2389, 2023.

[40] M. K. Chen, X. Y. Liu, Y. F. Wu, *et al*., "A meta-device for intelligent depth perception," *Advanced Materials*, in press.

[41] M. K. Chen, C. H. Chu, X. Y. Liu, *et al*., "Meta-lens in the sky," *IEEE Access*, vol. 10, pp. 46552–46557, 2022.

[42] M. Khorasaninejad, W. T. Chen, R. C. Devlin, *et al*., "Metalenses at visible wavelengths: Diffraction-limited focusing and subwavelength resolution imaging," *Science*, vol. 352, no. 6290, pp. 1190–1194, 2016.

[43] X. Y. Che, R. Gao, Y. F. Yu, *et al*., "Generalized phase profile design method for tunable devices using bilayer metasurfaces," *Optics Express*, vol. 29, no. 26, pp. 44214–44226, 2021.

[44] S. M. Wang, P. C. Wu, V. C. Su, *et al*., "Broadband achromatic optical metasurface devices," *Nature Communications*, vol. 8, no. 1, article no. 187, 2017.

[45] X. Y. Che, Y. F. Yu, Z. S. Gao, *et al*., "A broadband achromatic Alvarez metalens," *Optics & Laser Technology*, vol. 159, article no. 108985, 2023.

[46] S. M. Wang, P. C. Wu, V. C. Su, *et al*., "A broadband achromatic metalens in the visible," *Nature Nanotechnology*, vol. 13, no. 3, pp. 227–232, 2018.

[47] L. Li, Z. X. Liu, X. F. Ren, *et al*., "Metalens-array-based high-dimensional and multiphoton quantum source," *Science*, vol. 368, no. 6498, pp. 1487–1490, 2020.

[48] J. Karst, M. Floess, M. Ubl, *et al*., "Electrically switchable metallic polymer nanoantennas," *Science*, vol. 374, no. 6567, pp. 612–616, 2021.

[49] P. Yu, J. X. Li, and N. Liu, "Electrically tunable optical metasurfaces for dynamic polarization conversion," *Nano Letters*, vol. 21, no. 15, pp. 6690–6695, 2021.

[50] W. H. Yang, S. M. Xiao, Q. H. Song, *et al*., "All-dielectric metasurface for high-performance structural color," *Nature Communications*, vol. 11, no. 1, article no. 1864, 2020.

[51] R. Kaissner, J. X. Li, W. Z. Lu, *et al*., "Electrochemically controlled metasurfaces with high-contrast switching at visible frequencies," *Science Advances*, vol. 7, no. 19, article no. eabd9450, 2021.

[52] Y. Liang, K. Koshelev, F. C. Zhang, *et al*., "Bound states in the continuum in anisotropic plasmonic metasurfaces," *Nano Letters*, vol. 20, no. 9, pp. 6351–6356, 2020.

[53] Y. Liang, H. Lin, S. R. Lin, *et al*., "Hybrid anisotropic plasmonic metasurfaces with multiple resonances of focused light beams," *Nano Letters*, vol. 21, no. 20, pp. 8917–8923, 2021.

[54] T. Lei, M. Zhang, Y. R. Li, *et al*., "Massive individual orbital angular momentum channels for multiplexing enabled by Dammann

gratings," *Light:Science & Applications*, vol. 4, no. 3, article no. e257, 2015.

[55] R. J. Lin, V. C. Su, S. M. Wang, *et al*., "Achromatic metalens array for full-colour light-field imaging," *Nature Nanotechnology*, vol. 14, no. 3, pp. 227–231, 2019.

[56] S. Colburn, A. Zhan, and A. Majumdar, "Varifocal zoom imaging with large area focal length adjustable metalenses," *Optica*, vol. 5, no. 7, pp. 825–831, 2018.

[57] L. L. Huang, X. Z. Chen, H. Mühlenbernd, *et al*., "Dispersionless phase discontinuities for controlling light propagation," *Nano Letters*, vol. 12, no. 11, pp. 5750–5755, 2012.

[58] A. Arbabi, Y. Horie, M. Bagheri, *et al*., "Dielectric metasurfaces for complete control of phase and polarization with subwavelength spatial resolution and high transmission," *Nature Nanotechnology*, vol. 10, no. 11, pp. 937–943, 2015.

[59] P. C. Wu, W. Y. Tsai, W. T. Chen, *et al*., "Versatile polarization generation with an aluminum plasmonic metasurface," *Nano Letters*, vol. 17, no. 1, pp. 445–452, 2017.

[60] C. Yan, X. Li, M. B. Pu, *et al*., "Midinfrared real-time polarization imaging with all-dielectric metasurfaces," *Applied Physics Letters*, vol. 114, no. 16, article no. 161904, 2019.

[61] S. Wang, Z. L. Deng, Y. J. Wang, *et al*., "Arbitrary polarization conversion dichroism metasurfaces for all-in-one full Poincaré sphere polarizers," *Light:Science & Applications*, vol. 10, no. 1, article no. 24, 2021.

[62] L. Q. Cong, Y. K. Srivastava, H. F. Zhang, *et al*., "All-optical active THz metasurfaces for ultrafast polarization switching and dynamic beam splitting," *Light:Science & Applications*, vol. 7, article no. 28, 2018.

[63] P. C. Wu, R. Sokhoyan, G. K. Shirmanesh, *et al*., "Near-infrared active metasurface for dynamic polarization conversion," *Advanced Optical Materials*, vol. 9, no. 16, article no. 2100230, 2021.

[64] B. Xiong, Y. Liu, Y. H. Xu, *et al*., "Breaking the limitation of polarization multiplexing in optical metasurfaces with engineered noise," *Science*, vol. 379, no. 6629, pp. 294–299, 2023.

[65] G. Zograf, K. Koshelev, A. Zalogina, *et al*., "High-harmonic generation from resonant dielectric metasurfaces empowered by bound states in the continuum," *ACS Photonics*, vol. 9, no. 2, pp. 567–574, 2022.

[66] X. G. Zhang, Y. L. Sun, B. C. Zhu, *et al*., "A metasurface-based light-to-microwave transmitter for hybrid wireless communications," *Light:Science & Applications*, vol. 11, no. 1, article no. 126, 2022.

[67] K. C. Shen, C. T. Ku, C. Hsieh, *et al*., "Deep-ultraviolet hyperbolic metacavity laser," *Advanced Materials*, vol. 30, no. 21, article no. 1706918, 2018.

[68] W. Y. Tsai, T. L. Chung, H. H. Hsiao, *et al*., "Second harmonic light manipulation with vertical split ring resonators," *Advanced Materials*, vol. 31, no. 7, article no. 1806479, 2019.

[69] J. Jang, T. Badloe, Y. Yang, *et al*., "Spectral modulation through the hybridization of mie-scatterers and quasi-guided mode resonances: Realizing full and gradients of structural color," *ACS Nano*, vol. 14, no. 11, pp. 15317–15326, 2020.

[70] Y. K. Wu, W. H. Yang, Y. B. Fan, *et al*., "Tio$_2$ metasurfaces: From visible planar photonics to photochemistry," *Science Advances*, vol. 5, no. 11, article no. eaax0939, 2019.

[71] S. Sun, W. H. Yang, C. Zhang, *et al*., "Real-time tunable colors from microfluidic reconfigurable all-dielectric metasurfaces," *ACS Nano*, vol. 12, no. 3, pp. 2151–2159, 2018.

[72] J. Yao, G. X. Cai, N. Liu, *et al*., "Enhancing artificial sum frequency generation from graphene-gold metamolecules," *Optics Letters*, vol. 43, no. 13, pp. 3160–3163, 2018.

[73] J. Yao, Y. N. Wu, J. Liu, *et al*., "Enhanced optical bistability by coupling effects in magnetic metamaterials," *Journal of Lightwave Technology*, vol. 37, no. 23, pp. 5814–5820, 2019.

[74] S. Sun, Z. X. Zhou, C. Zhang, *et al*., "All-dielectric full-color printing with TiO$_2$ metasurfaces," *ACS Nano*, vol. 11, no. 5, pp. 4445–4452, 2017.

[75] T. Badloe, J. Kim, I. Kim, *et al*., "Liquid crystal-powered mie resonators for electrically tunable photorealistic color gradients and dark blacks," *Light:Science & Applications*, vol. 11, no. 1, article no. 118, 2022.

[76] X. L. Liu, T. Tyler, T. Starr, *et al*., "Taming the blackbody with infrared metamaterials as selective thermal emitters," *Physical Review Letters*, vol. 107, no. 4, article no. 045901, 2011.

[77] L. Zhou, Y. L. Tan, D. X. Ji, *et al*., "Self-assembly of highly efficient, broadband plasmonic absorbers for solar steam generation," *Science Advances*, vol. 2, no. 4, article no. e1501227, 2016.

[78] V. G. Kravets, A. V. Kabashin, W. L. Barnes, *et al*., "Plasmonic surface lattice resonances: A review of properties and applications," *Chemical Reviews*, vol. 118, no. 12, pp. 5912–5951, 2018.

[79] C. M. Watts, X. L. Liu, and W. J. Padilla, "Metamaterial electromagnetic wave absorbers," *Advanced Materials*, vol. 24, no. 23, pp. OP98–OP120, 2012.

[80] N. I. Landy, S. Sajuyigbe, J. J. Mock, *et al*., "Perfect metamaterial absorber," *Physical Review Letters*, vol. 100, no. 20, article no. 207402, 2008.

[81] N. Liu, M. Mesch, T. Weiss, *et al*., "Infrared perfect absorber and its application as plasmonic sensor," *Nano Letters*, vol. 10, no. 7, pp. 2342–2348, 2010.

[82] X. Xiong, S. C. Jiang, Y. H. Hu, *et al*., "Structured metal film as a perfect absorber," *Advanced Materials*, vol. 25, no. 29, pp. 3994–4000, 2013.

[83] R. Masoudian Saadabad, L. J. Huang, and A. E. Miroshnichenko, "Polarization-independent perfect absorber enabled by quasi-bound states in the continuum," *Physical Review B*, vol. 104, no. 23, article no. 235405, 2021.

[84] X. Y. Zheng, J. Lin, Z. Wang, *et al*., "Manipulating light transmission and absorption via an achromatic reflectionless metasurface," *PhotoniX*, vol. 4, no. 1, article no. 3, 2023.

[85] A. Leitis, A. Tittl, M. K. Liu, *et al*., "Angle-multiplexed all-dielectric metasurfaces for broadband molecular fingerprint retrieval," *Science Advances*, vol. 5, no. 5, article no. eaaw2871, 2019.

[86] A. Tittl, A. Leitis, M. K. Liu, *et al*., "Imaging-based molecular barcoding with pixelated dielectric metasurfaces," *Science*, vol. 360, no. 6393, pp. 1105–1109, 2018.

[87] S. K. Deng, R. Li, J. E. Park, *et al*., "Ultranarrow plasmon resonances from annealed nanoparticle lattices," *Proceedings of the National Academy of Sciences of the United States of America*, vol. 117, no. 38, pp. 23380–23384, 2020.

[88] S. K. Deng, J. E. Park, G. Kang, *et al*., "Interfacial engineering of plasmonic nanoparticle metasurfaces," *Proceedings of the National Academy of Sciences of the United States of America*, vol. 119, no. 22, article no. e2202621119, 2022.

[89] F. Costa, S. Genovesi, A. Monorchio, *et al*., "A circuit-based model for the interpretation of perfect metamaterial absorbers," *IEEE Transactions on Antennas and Propagation*, vol. 61, no. 3, pp. 1201–1209, 2013.

[90] L. Zhou, Y. L. Tan, J. Y. Wang, *et al*., "3D self-assembly of aluminium nanoparticles for plasmon-enhanced solar desalination," *Nature Photonics*, vol. 10, no. 6, pp. 393–398, 2016.

[91] K. Chen, R. Adato, and H. Altug, "Dual-band perfect absorber for multispectral plasmon-enhanced infrared spectroscopy," *ACS*

Nano, vol. 6, no. 9, pp. 7998–8006, 2012.

[92] A. K. Yang, Z. Y. Li, M. P. Knudson, *et al*., "Unidirectional lasing from template-stripped two-dimensional plasmonic crystals," *ACS Nano*, vol. 9, no. 12, pp. 11582–11588, 2015.

[93] F. Cheng, J. Gao, T. S. Luk, *et al*., "Structural color printing based on plasmonic metasurfaces of perfect light absorption," *Scientific Reports*, vol. 5, article no. 11045, 2015.

[94] A. Tittl, A. K. U. Michel, M. Schäferling, *et al*., "A switchable mid-infrared plasmonic perfect absorber with multispectral thermal imaging capability," *Advanced Materials*, vol. 27, no. 31, pp. 4597–4603, 2015.

[95] L. Allen, M. W. Beijersbergen, R. J. C. Spreeuw, *et al*., "Orbital angular momentum of light and the transformation of laguerre-gaussian laser modes," *Physical Review A*, vol. 45, no. 11, pp. 8185–8189, 1992.

[96] Y. X. Cao, S. Yan, W. D. Liu, *et al*., "Generation of multi-OAM beams using a compact dual-mode source and a 3d-printed luneburg lens," *Optics Express*, vol. 30, no. 23, pp. 41181–41195, 2022.

[97] J. Wang, J. Y. Yang, I. M. Fazal, *et al*., "Terabit free-space data transmission employing orbital angular momentum multiplexing," *Nature Photonics*, vol. 6, no. 7, pp. 488–496, 2012.

[98] G. B. Wu, K. F. Chan, K. M. Shum, *et al*., "Millimeter-wave holographic flat lens antenna for orbital angular momentum multiplexing," *IEEE Transactions on Antennas and Propagation*, vol. 69, no. 8, pp. 4289–4303, 2021.

[99] G. B. Wu, K. F. Chan, S. W. Qu, *et al*., "Orbital angular momentum (OAM) mode-reconfigurable discrete dielectric lens operating at 300 GHz," *IEEE Transactions on Terahertz Science and Technology*, vol. 10, no. 5, pp. 480–489, 2020.

[100] R. X. Zheng, R. H. Pan, G. Z. Geng, *et al*., "Active multiband varifocal metalenses based on orbital angular momentum division multiplexing," *Nature Communications*, vol. 13, no. 1, article no. 4292, 2022.

[101] Y. H. Guo, S. C. Zhang, M. B. Pu, *et al*., "Spin-decoupled metasurface for simultaneous detection of spin and orbital angular momenta via momentum transformation," *Light:Science & Applications*, vol. 10, no. 1, article no. 63, 2021.

[102] Y. J. Shen, X. J. Wang, Z. W. Xie, *et al*., "Optical vortices 30 years on: OAM manipulation from topological charge to multiple singularities," *Light:Science & Applications*, vol. 8, article no. 90, 2019.

[103] M. W. Song, L. Feng, P. C. Huo, *et al*., "Versatile full-colour nanopainting enabled by a pixelated plasmonic metasurface," *Nature Nanotechnology*, vol. 18, no. 1, pp. 71–78, 2023.

[104] M. V. Rybin, K. L. Koshelev, Z. F. Sadrieva, *et al*., "High-*Q* supercavity modes in subwavelength dielectric resonators," *Physical Review Letters*, vol. 119, no. 24, article no. 243901, 2017.

[105] C. W. Hsu, B. Zhen, J. Lee, *et al*., "Observation of trapped light within the radiation continuum," *Nature*, vol. 499, no. 7457, pp. 188–191, 2013.

[106] C. W. Hsu, B. Zhen, A. D. Stone, *et al*., "Bound states in the continuum," *Nature Reviews Materials*, vol. 1, no. 9, article no. 16048, 2016.

[107] K. Koshelev, S. Lepeshov, M. K. Liu, *et al*., "Asymmetric metasurfaces with high-*Q* resonances governed by bound states in the continuum," *Physical Review Letters*, vol. 121, no. 19, article no. 193903, 2018.

[108] S. I. Azzam, V. M. Shalaev, A. Boltasseva, *et al*., "Formation of bound states in the continuum in hybrid plasmonic-photonic systems," *Physical Review Letters*, vol. 121, no. 25, article no. 253901, 2018.

[109] X. D. Zhang, Y. L. Liu, J. C. Han, *et al*., "Chiral emission from resonant metasurfaces," *Science*, vol. 377, no. 6611, pp. 1215–1218, 2022.

[110] Y. Chen, H. C. Deng, X. B. Sha, *et al*., "Observation of intrinsic chiral bound states in the continuum," *Nature*, vol. 613, no. 7944, pp. 474–478, 2023.

[111] Y. H. Tang, Y. Liang, J. Yao, *et al*., "Chiral bound states in the continuum in plasmonic metasurfaces," *Laser & Photonics Reviews*, vol. 17, no. 4, article no. 2200597, 2023.

[112] Y. Liang, H. Lin, K. Koshelev, *et al*., "Full-stokes polarization perfect absorption with diatomic metasurfaces," *Nano Letters*, vol. 21, no. 2, pp. 1090–1095, 2021.

[113] K. Koshelev, Y. T. Tang, Z. X. Hu, *et al*., "Resonant chiral effects in nonlinear dielectric metasurfaces," *ACS Photonics*, vol. 10, no. 1, pp. 298–306, 2023.

[114] T. Shi, Z. L. Deng, G. Z. Geng, *et al*., "Planar chiral metasurfaces with maximal and tunable chiroptical response driven by bound states in the continuum," *Nature Communications*, vol. 13, no. 1, article no. 4111, 2022.

[115] G. Y. Lee, G. Yoon, S. Y. Lee, *et al*., "Complete amplitude and phase control of light using broadband holographic metasurfaces," *Nanoscale*, vol. 10, no. 9, pp. 4237–4245, 2018.

[116] A. C. Overvig, S. Shrestha, S. C. Malek, *et al*., "Dielectric metasurfaces for complete and independent control of the optical amplitude and phase," *Light:Science & Applications*, vol. 8, article no. 92, 2019.

[117] J. Y. Dai, J. Zhao, Q. Cheng, *et al*., "Independent control of harmonic amplitudes and phases via a time-domain digital coding metasurface," *Light:Science & Applications*, vol. 7, article no. 90, 2018.

[118] M. Farsari and B. N. Chichkov, "Two-photon fabrication," *Nature Photonics*, vol. 3, no. 8, pp. 450–452, 2009.

[119] X. J. Ni, A. V. Kildishev, and V. M. Shalaev, "Metasurface holograms for visible light," *Nature Communications*, vol. 4, no. 1, article no. 2807, 2013.

[120] L. X. Liu, X. Q. Zhang, M. Kenney, *et al*., "Broadband metasurfaces with simultaneous control of phase and amplitude," *Advanced Materials*, vol. 26, no. 29, pp. 5031–5036, 2014.

[121] W. J. Sun, Q. He, S. L. Sun, *et al*., "High-efficiency surface plasmon meta-couplers: Concept and microwave-regime realizations," *Light:Science & Applications*, vol. 5, no. 1, article no. e16003, 2016.

[122] T. Cai, G. M. Wang, S. W. Tang, *et al*., "High-efficiency and full-space manipulation of electromagnetic wave fronts with metasurfaces," *Physical Review Applied*, vol. 8, no. 3, article no. 034033, 2017.

[123] Q. He, S. L. Sun, S. Y. Xiao, *et al*., "High-efficiency metasurfaces: Principles, realizations, and applications," *Advanced Optical Materials*, vol. 6, no. 19, article no. 1800415, 2018.

[124] C. Pfeiffer and A. Grbic, "Metamaterial huygens' surfaces: Tailoring wave fronts with reflectionless sheets," *Physical Review Letters*, vol. 110, no. 19, article no. 197401, 2013.

[125] J. Lin, P. Genevet, M. A. Kats, *et al*., "Nanostructured holograms for broadband manipulation of vector beams," *Nano Letters*, vol. 13, no. 9, pp. 4269–4274, 2013.

[126] D. Y. Wang, F. F. Liu, T. Liu, *et al*., "Efficient generation of complex vectorial optical fields with metasurfaces," *Light:Science & Applications*, vol. 10, no. 1, article no. 67, 2021.

[127] D. Y. Wang, T. Liu, Y. J. Zhou, *et al*., "High-efficiency metadevices for bifunctional generations of vectorial optical fields," *Nanophotonics*, vol. 10, no. 1, pp. 685–695, 2020.

[128] F. F. Liu, D. Y. Wang, H. Zhu, *et al*., "High-efficiency metasurface-based surface-plasmon lenses," *Laser & Photonics Reviews*, vol. 17, no. 7, article no. 2201001, 2023.

[129] W. T. Chen, K. Y. Yang, C. M. Wang, *et al*., "High-efficiency broadband meta-hologram with polarization-controlled dual images," *Nano Letters*, vol. 14, no. 1, pp. 225–230, 2014.

[130] T. Cai, S. W. Tang, G. M. Wang, *et al*., "High-performance bifunctional metasurfaces in transmission and reflection geometries," *Advanced Optical Materials*, vol. 5, no. 2, article no. 1600506, 2017.

[131] S. Q. Li, Z. Wang, S. H. Dong, *et al*., "Helicity-delinked manipulations on surface waves and propagating waves by metasurfaces," *Nanophotonics*, vol. 9, no. 10, pp. 3473–3481, 2020.

[132] Z. Wang, S. Q. Li, X. Q. Zhang, *et al*., "Excite spoof surface plasmons with tailored wavefronts using high-efficiency terahertz metasurfaces," *Advanced Science*, vol. 7, no. 19, article no. 2000982, 2020.

[133] Z. Wang, Y. Yao, W. K. Pan, *et al*., "Bifunctional manipulation of terahertz waves with high-efficiency transmissive dielectric metasurfaces," *Advanced Science*, vol. 10, no. 4, article no. 2205499, 2023.

[134] E. Arbabi, S. M. Kamali, A. Arbabi, *et al*., "Full-stokes imaging polarimetry using dielectric metasurfaces," *ACS Photonics*, vol. 5, no. 8, pp. 3132–3140, 2018.

[135] Z. C. Shen, F. Zhao, C. Q. Jin, *et al*., "Monocular metasurface camera for passive single-shot 4D imaging," *Nature Communications*, vol. 14, no. 1, article no. 1035, 2023.

[136] X. F. Zang, H. Z. Ding, Y. Intaravanne, *et al*., "A multi-foci metalens with polarization-rotated focal points," *Laser & Photonics Reviews*, vol. 13, no. 12, article no. 1900182, 2019.

[137] M. Khorasaninejad, W. T. Chen, A. Y. Zhu, *et al*., "Multispectral chiral imaging with a metalens," *Nano Letters*, vol. 16, no. 7, pp. 4595–4600, 2016.

[138] Z. L. Deng, J. H. Deng, X. Zhuang, *et al*., "Diatomic metasurface for vectorial holography," *Nano Letters*, vol. 18, no. 5, pp. 2885–2892, 2018.

[139] W. P. Wan, W. H. Yang, H. Feng, *et al*., "Multiplexing vectorial holographic images with arbitrary metaholograms," *Advanced Optical Materials*, vol. 9, no. 20, article no. 2100626, 2021.

[140] J. P. Balthasar Mueller, N. A. Rubin, R. C. Devlin, *et al*., "Metasurface polarization optics: Independent phase control of arbitrary orthogonal states of polarization," *Physical Review Letters*, vol. 118, no. 11, article no. 113901, 2017.

[141] M. Kauranen and A. V. Zayats, "Nonlinear plasmonics," *Nature Photonics*, vol. 6, no. 11, pp. 737–748, 2012.

[142] M. Celebrano, X. F. Wu, M. Baselli, *et al*., "Mode matching in multiresonant plasmonic nanoantennas for enhanced second harmonic generation," *Nature Nanotechnology*, vol. 10, no. 5, pp. 412–417, 2015.

[143] J. Lee, M. Tymchenko, C. Argyropoulos, *et al*., "Giant nonlinear response from plasmonic metasurfaces coupled to intersubband transitions," *Nature*, vol. 511, no. 7507, pp. 65–69, 2014.

[144] Y. M. Yang, W. Y. Wang, A. Boulesbaa, *et al*., "Nonlinear fano-resonant dielectric metasurfaces," *Nano Letters*, vol. 15, no. 11, pp. 7388–7393, 2015.

[145] L. Wang, S. Kruk, K. Koshelev, *et al*., "Nonlinear wavefront control with all-dielectric metasurfaces," *Nano Letters*, vol. 18, no. 6, pp. 3978–3984, 2018.

[146] J. Y. Dai, L. X. Yang, J. C. Ke, *et al*., "High-efficiency synthesizer for spatial waves based on space-time-coding digital metasurface," *Laser & Photonics Reviews*, vol. 14, no. 6, article no. 1900133, 2020.

[147] Z. N. Wu and A. Grbic, "Serrodyne frequency translation using time-modulated metasurfaces," in *Proceedings of the IEEE International Symposium on Antennas and Propagation and Usnc-Ursi Radio Science Meeting*, Atlanta, GA, USA, pp.1609–1610, 2019.

[148] L. Zhang, X. Q. Chen, S. Liu, *et al*., "Space-time-coding digital metasurfaces," *Nature Communications*, vol. 9, no. 1, article no. 4334, 2018.

[149] L. Zhang, M. Z. Chen, W. K. Tang, *et al*., "A wireless communication scheme based on space- and frequency-division multiplexing using digital metasurfaces," *Nature Electronics*, vol. 4, no. 3, pp. 218–227, 2021.

[150] Y. Hadad, J. C. Soric, and A. Alu, "Breaking temporal symmetries for emission and absorption," *Proceedings of the National Academy of Sciences of the United States of America*, vol. 113, no. 13, pp. 3471–3475, 2016.

[151] X. X. Guo, Y. M. Ding, Y. Duan, *et al*., "Nonreciprocal metasurface with space-time phase modulation," *Light:Science & Applications*, vol. 8, no. 1, article no. 123, 2019.

[152] G. B. Wu, J. Y. Dai, and C. H. Chan, "Four-dimensional (4-D) leaky-wave antenna for frequency translation," in *Proceedings of 2022 Asia-Pacific Microwave Conference*, Yokohama, Japan, pp.267–269, 2022.

[153] G. B. Wu, J. Y. Dai, and C. H. Chan, "Time-modulated leaky-wave antennas," in *Proceedings of 2022 IEEE International Symposium on Antennas and Propagation and USNC-URSI Radio Science Meeting*, Denver, CO, USA, pp.812–813, 2022.

[154] M. L. Tseng, M. Semmlinger, M. Zhang, *et al*., "Vacuum ultraviolet nonlinear metalens," *Science Advances*, vol. 8, no. 16, article no. eabn5644, 2022.

[155] J. X. Zhou, J. X. Zhao, Q. Y. Wu, *et al*., "Nonlinear computational edge detection metalens," *Advanced Functional Materials*, vol. 32, no. 34, article no. 2204734, 2022.

[156] G. X. Li, S. Zhang, and T. Zentgraf, "Nonlinear photonic metasurfaces," *Nature Reviews Materials*, vol. 2, no. 5, article no. 17010, 2017.

[157] M. Z. Liu, W. Q. Zhu, P. C. Huo, *et al*., "Multifunctional metasurfaces enabled by simultaneous and independent control of phase and amplitude for orthogonal polarization states," *Light:Science & Applications*, vol. 10, no. 1, article no. 107, 2021.

[158] Y. J. Bao, L. Wen, Q. Chen, *et al*., "Toward the capacity limit of 2D planar jones matrix with a single-layer metasurface," *Science Advances*, vol. 7, no. 25, article no. eabh0365, 2021.

[159] S. F. Zhang, L. L. Huang, X. Li, *et al*., "Dynamic display of full-stokes vectorial holography based on metasurfaces," *ACS Photonics*, vol. 8, no. 6, pp. 1746–1753, 2021.

[160] C. Chen, X. Ye, J. C. Sun, *et al*., "Bifacial-metasurface-enabled pancake metalens with polarized space folding," *Optica*, vol. 9, no. 12, pp. 1314–1322, 2022.

[161] S. C. Malek, A. C. Overvig, A. Alù, *et al*., "Multifunctional resonant wavefront-shaping meta-optics based on multilayer and multiperturbation nonlocal metasurfaces," *Light:Science & Applications*, vol. 11, no. 1, article no. 246, 2022.

[162] X. Y. Guo, J. Z. Zhong, B. J. Li, *et al*., "Full-color holographic display and encryption with full-polarization degree of freedom," *Advanced Materials*, vol. 34, no. 3, article no. 2103192, 2022.

[163] A. Overvig, N. F. Yu, and A. Alù, "Chiral quasi-bound states in the continuum," *Physical Review Letters*, vol. 126, no. 7, article no. 073001, 2021.

[164] Y. Q. Hu, L. Li, Y. J. Wang, *et al*., "Trichromatic and tripolarization-channel holography with noninterleaved dielectric metasurface," *Nano Letters*, vol. 20, no. 2, pp. 994–1002, 2020.

[165] Q. H. Song, A. Baroni, R. Sawant, *et al*., "Ptychography retrieval of fully polarized holograms from geometric-phase metasurfaces," *Nature Communications*, vol. 11, no. 1, article no. 2651, 2020.

[166] Z. L. Deng, M. K. Jin, X. Ye, *et al*., "Full-color complex-amplitude vectorial holograms based on multi-freedom metasurfaces," *Advanced Functional Materials*, vol. 30, no. 21, article no. 1910610, 2020.

[167] N. A. Rubin, G. D'aversa, P. Chevalier, *et al*., "Matrix Fourier optics enables a compact full-stokes polarization camera," *Science*, vol. 365, no. 6448, article no. eaax1839, 2019.

[168] X. Ye, X. Qian, Y. X. Chen, *et al*., "Chip-scale metalens microscope for wide-field and depth-of-field imaging," *Advanced Photonics*, vol. 4, no. 4, article no. 046006, 2022.

[169] M. K. Chen, Y. F. Wu, L. Feng, *et al*., "Principles, functions, and applications of optical meta-lens," *Advanced Optical Materials*, vol. 9, no. 4, article no. 2001414, 2021.

Jing Cheng Zhang received the M.S. degree in electronic information engineering from Northwestern Polytechnical University, Xi'an, China, in 2019. He is currently working toward the Ph.D. degree in electrical engineering at City University of Hong Kong, Hong Kong, China. He has published several peer-reviewed papers in prestigious journals, including *Science Advances*. His current research interests include metasurfaces, metalens arrays, and applications of quantum optics and metadevices.
(Email: jzhang2442-c@my.cityu.edu.hk)

Geng-Bo Wu received the B.S. and M.S. degrees from the University of Electronic Science and Technology of China, Chengdu, China, in 2015 and 2018, respectively, and Ph.D. degree from the City University of Hong Kong (CityU), Hong Kong, in 2021. He is now a Postdoctoral Research Fellow with the State Key Laboratory of Terahertz and Millimeter Waves, CityU. He has published more than 30 peer-reviewed papers in prestigious journals, including *Nature Electronics*, *Science Advances*, and *IEEE Transactions* series. His research interests include millimeter-wave/THz antennas, metasurfaces, and their applications in imaging and wireless communications.
(Email: bogwu2@cityu.edu.hk)

Mu Ku Chen received the Ph.D. degree from the Department of Physics at the Chinese Taiwan University in 2019. He was a Research Assistant Professor in the Department of Electronic and Information Engineering at The Hong Kong Polytechnic University. At present, he is an Assistant Professor of the Department of Electrical Engineering at City University of Hong Kong. His research interests include photonic information, nanophotonics, micro&nano-electronics fabrication, and artificial nano-antenna array-based meta-devices for photonic applications.
(Email: mkchen@cityu.edu.hk)
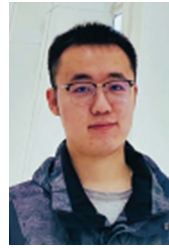
Xiaoyu Che received the B.S. degree from the Nanjing University of Science and Technology, China, in 2019. He is currently a Ph.D. student in the School of Electronic and Optic Engineering, Nanjing University of Science and Technology, and a visiting research student in the Department of Electrical Engineering, City University of Hong Kong. His current research interests include meta-devices, optical system design and application.
(Email: xyche2-c@my.cityu.edu.hk)

Yao Liang received the Ph.D. degree from the Centre for Translational Atomaterials at the Swinburne University of Technology in 2020. He is a Postdoc Researcher at the Department of Electrical Engineering at the City University of Hong Kong. His research interests include plasmonics, bound states in the continuum, surface lattice resonances, integrated photonics, and functional meta-devices.
(Email: yaoliang@cityu.edu.hk)
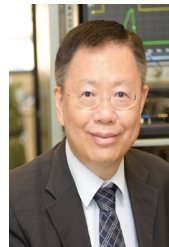
Din Ping Tsai received the Ph.D. degree from the University of Cincinnati, USA, in 1990. He is currently Chair Professor of the Department of Electrical Engineering, City University of Hong Kong. He is an elected Fellow of AAAS, APAM, APS, COS, EMA, IAE, IEEE, JSAP, NAI, OSA, SPIE, and TPS. He received more than 40 prestigious recognitions and awards, including "Global Highly Cited Researchers" and Web of Science Group (Clarivate Analytics) in 2020 and 2019, respectively; China's Top 10 Optical Breakthroughs in 2020 and 2018; and the "Mozi Award" from the International Society for Optics and Photonics (SPIE) (2018).
(Email: dptsai@cityu.edu.hk)

Chi Hou Chan received the Ph.D. degree in electrical engineering from the University of Illinois, Urbana, IL, USA, in 1987. In 1996, he joined the Department of Electronic Engineering (now Electrical Engineering), City University of Hong Kong (CityU), as Professor and was promoted to Chair Professor of Electronic Engineering in 1998. He is currently the Director of the State Key Laboratory of Terahertz and Millimeter Waves (City University of Hong Kong). His current research interests include computational electromagnetics, millimeter-wave circuits and antennas, and terahertz science and technology.

Professor Chan was elected an IEEE Fellow in 2002. He received the 2019 IEEE Antennas and Propagation Society Harrington-Mittra Computational Electromagnetics Award and the 2019 Distinguished Alumni Award from the Department of Electrical and Computer Engineering, University of Illinois at Urbana-Champaign.
(Email: eechic@cityu.edu.hk)